Modelling an upend hinge in hydrodynamic simulations of a monopile upend operation

MSc Thesis

Dylan J. van Rooijen

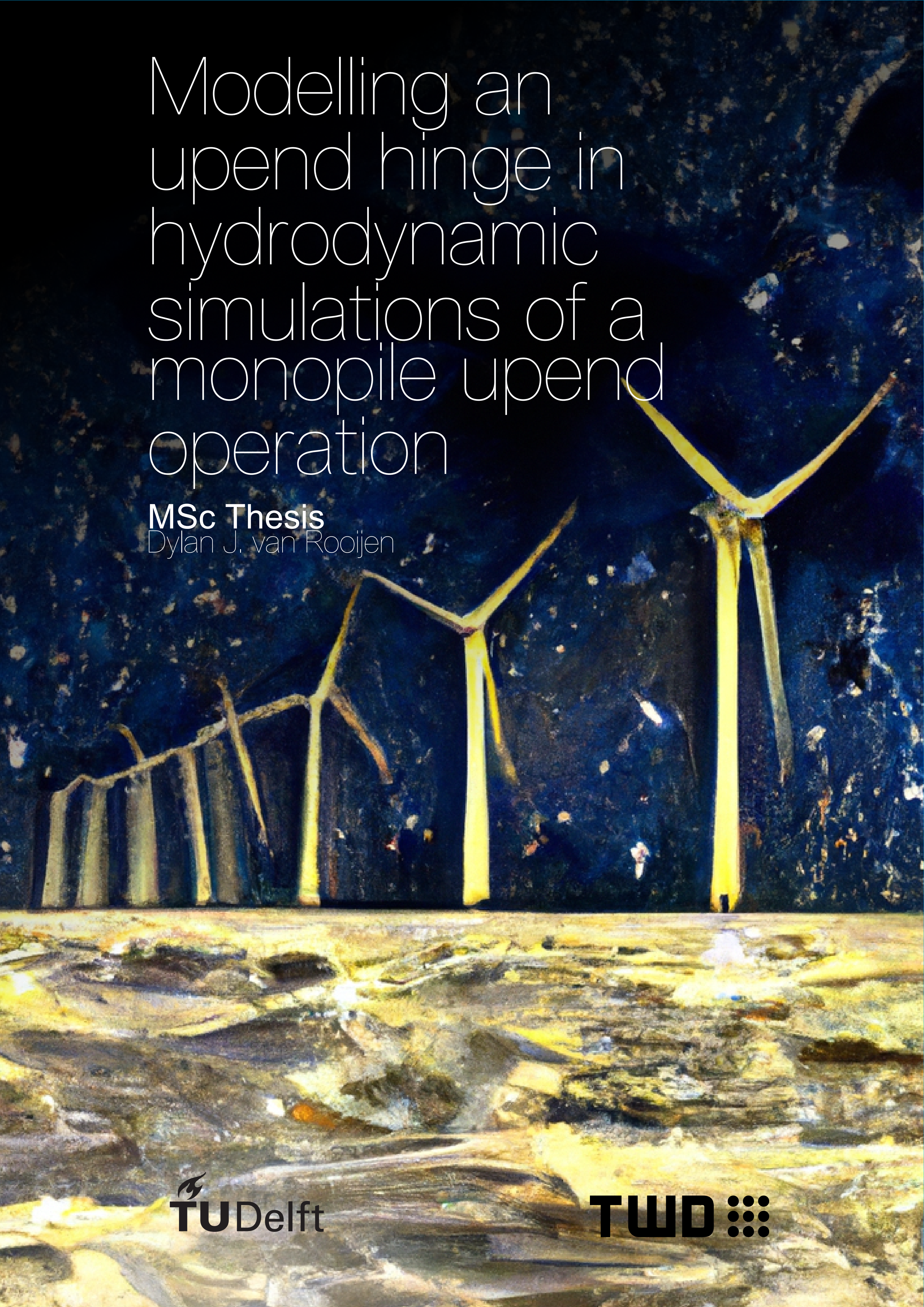

Cover image generated using DALL·E 2 by OpenAI

Modelling an upend hinge in hydrodynamic simulations of a monopile upend operation

MSc Thesis

by

Dylan J. van Rooijen

Student number: 4543378
Thesis committee: **Chair:** Prof.dr. A. Metrikine
Supervisor TU Delft: Dr. E. Lourens
Supervisor TWD: Ir. J.B. van Wuijckhuijse
4th member: Dr. A. Cabboi
5th member: Dr.ir. K.N. van Dalen

Abstract

As the offshore wind energy industry is growing, so are the wind turbines and the monopile foundations on which they are built. As these monopile foundations grow, the installation operations become more critical. To ensure that the operability of these operations can be accurately determined, TWD is interested in applying Dynamic Substructuring to more accurately model an upend hinge in upending operations. This thesis aims to outline the application of Dynamic Substructuring to an upend hinge. Furthermore, the resulting model is compared with a conventional model to assess the viability of the application of Dynamic Substructuring for modelling an upend hinge.

The resulting model has a significantly different dynamic behaviour than the conventional model. This difference, however, is mainly in the high-frequency spectrum. As an upend hinge operates mainly in relatively low frequent waves, this difference is minimally relevant. When subjected to typical ocean wave frequencies, there is very little difference between the dynamic behaviour of the conventional model and the substructured model. The computation time of the simulations using Dynamic Substructuring, however, is roughly 10 times higher than the conventional simulations. Therefore, it is not recommended to apply dynamic substructuring to model this upend hinge in operability studies. For situations where the high-frequency response is more relevant, however, dynamic substructuring may prove a valuable tool to more accurately describe the dynamic properties of an upend hinge or other marine equipment.

Preface

> Pray look better, Sir... those things yonder are no giants, but windmills.
>
> Miguel de Cervantes

The report before you marks the end of my academic career at the TU Delft. I look back at my time graduating with a sense of relief and gratefulness. I am relieved because when I started in December, writing an MSc. thesis seemed like a daunting task. However, as I look back now, I can only describe it as a formative experience which was both challenging and rewarding. I am grateful to everyone who helped to bring this graduation to a successful end. There are several people I want to thank in particular.

First of all, I would like to express my gratitude to professors Metrikine and Lourens. Throughout the process, their insights helped me immensely to keep on track and move forward. Furthermore, I would like to thank Bas van Wuijckhuijse, who always had time to decipher my chaotic ideas and condense them into something understandable and workable. Many thanks as well to the Marine Team at TWD. They provided a great environment in which I look forward to continuing to work. Finally, a big thank you to my girlfriend, family and friends. Without their encouragement and support, I would have not been able to complete my graduation successfully.

Delft, October 2023

Dylan J. van Rooijen

Contents

Nomenclature

Acronyms

CoG Centre of Gravity.

DoF Degree of Freedom.

FE Finite Element.

FEM Finite Element Method.

MAC Modal Assurance Criterion.

MDAS Marine Dynamic Analysis Software.

MP Monopile.

ODE Ordinary Differential Equation.

POD Proper Orthogonal Decomposition.

POM Proper Orthogonal Mode.

POMAC Proper Orthogonal Modal Assurance Criterion.

POV Proper Orthogonal Value.

RAO Response Amplitude Operator.

SVD Singular Value Decomposition.

UEH Upend Hinge.

List of Symbols

$\boldsymbol{B}$ Signed Boolean matrix that operates on DoFs on the boundary to ensure compatibility of the substructures.

$\boldsymbol{C}$ Damping matrix.

$\boldsymbol{I}$ Identity matrix.

$\boldsymbol{K}$ Stiffness matrix.

$\boldsymbol{L}$ Boolean localization matrix found by computing the nullspace of $\boldsymbol{B}$.

$\boldsymbol{M}$ Mass matrix.

$\boldsymbol{R}$ Reduction matrix.

$\boldsymbol{S}$ Static condensation matrix.

$\boldsymbol{f}$ External force vector.

$\boldsymbol{g}$ Coupling force vector.

$\boldsymbol{q}$ Vector containing the set of unique degrees of freedom.

$\boldsymbol{u}$ Displacement vector.

$\boldsymbol{\Sigma}$ Pseudo diagonal matrix containing singular values.

$\boldsymbol{\Phi}$ Matrix containing interface-fixed modes.

$\boldsymbol{\eta}$ Modal amplitude vector.

$\boldsymbol{\mu}$ Average of the snapshots of a time-varying signal.

$\boldsymbol{\xi}$ Unique generalized Degree of Freedom (DoF) vector.

$\boldsymbol{\varphi}$ Mode shape.

$\boldsymbol{\psi}$ Generalized DoF vector.

ω Natural frequency.

$\boldsymbol{U}$ Matrix of left singular vectors.

$\boldsymbol{V}$ Matrix of right singular vectors.

$\boldsymbol{X}$ Mean centered response matrix.

$\boldsymbol{Z}$ Response matrix.

1

Introduction

The offshore wind energy industry is quite literally reaching for the sky to meet the increasing demand (IRENA, 2022) for renewable energy in Europe. Offshore wind turbines are sprouting out of the waves off the coast of many European nations and their size is increasing rapidly (Bilgili et al., 2022). As the turbines become larger and the waters in which they are placed become deeper, the foundations that carry these behemoths must grow as well. The most frequently used foundation is the Monopile (MP) (*Offshore Wind in Europe - Key trends and statistics 2020*, 2021). Over the years, both the length and the diameter of these MPs have steadily increased (Sánchez et al., 2019). Installing MPs has, as a result of this, become more and more difficult.

1.1. Monopile upending

One aspect of the installation of MPs that has become more challenging is the upending of the MP. When the MPs are transported to the site of installation, they are sea-fastened to the deck in horizontal orientation. When they arrive, they need to be rotated to a vertical orientation for installation. This can be done with the aid of an Upend Hinge (UEH). An example of a UEH is shown in figure 1.1. Before describing the UEH in more detail, it is important to address the upending procedure as a whole.

Figure 1.1: Example of an Upend Hinge (TWD Japan, 2023)

The upending procedure begins when both the installation vessel and the MP have arrived at the location of installation. First, the MP is moved from its sea fastening on deck towards the UEH. If the MP is transported on the deck of the installation vessel, this is sometimes done by a skidding system that is installed on the vessel. Usually, however, the MP is lifted into the UEH with a crane. Once the bottom end of the MP is in place in the UEH, a lifting tool is connected to the top end of the MP. The crane cable is then connected to the lifting tool and the lifting tool is hoisted up. During the lift of the top of MP, the bottom of the MP remains supported in the UEH. Once the MP is almost vertical, it is lifted out of the UEH. It is then ready for installation.

It is important to note that the UEH does not provide any lifting power. Its sole function is to support the MP during the lifting procedure. Nevertheless, the UEH experiences significant loads due to the weight of the MP and the motions of both the vessel and the MP in the waves.

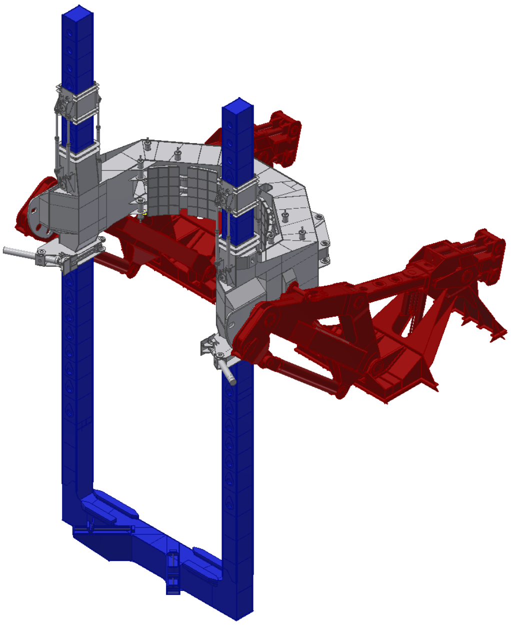

Figure 1.2: Model of a UEH with the folding frame in red, the bucket in grey and the U-frame in blue

Most UEHs consists of three distinctive components: the folding frame, the bucket and the U-frame. They are displayed in figure 1.2. The folding frame is the part of the UEH that connects it to the deck of the vessel. It may allow the UEH to fold away to improve clearance. The bucket is the crescent-shaped structure in which the MP lies when horizontal. The aptly named U-frame is the U-shaped structure that supports the MP when it is almost vertical. Although the connection point between the U-frame and the bucket may be adjustable to accommodate multiple pile lengths, during upending the connection between the U-frame and bucket is rigid. The connection between the bucket and the folding frame allows for rotation along one axis to facilitate the upending motion.

The UEH must be strong enough to be able to support the MP without failure. Furthermore, it must be stiff to limit crane wire angles and prevent excessive motions during the upending operation. There is, however, a limit to how stiff the hinge can realistically be. As MPs grow in size and more specifically get heavier, the flexibility of the hinge becomes a point of concern. The dynamic behaviour of the UEH during the upending operation is therefore interesting to investigate.

1.2. Operability simulations

The main reason for modelling the upending operation is to investigate operability. The objective, here, is to determine under which environmental conditions the operation can safely be performed. To this end, a numerical hydrodynamic model is constructed. The model consists of at least the installation vessel and the MP. Furthermore, usually, a mooring system for the ship is also modelled. The top of the MP is connected, through the crane wire, to the crane on the vessel. The bottom of the MP is connected to the vessel through the UEH. An example of such a model is shown in figure 1.3.

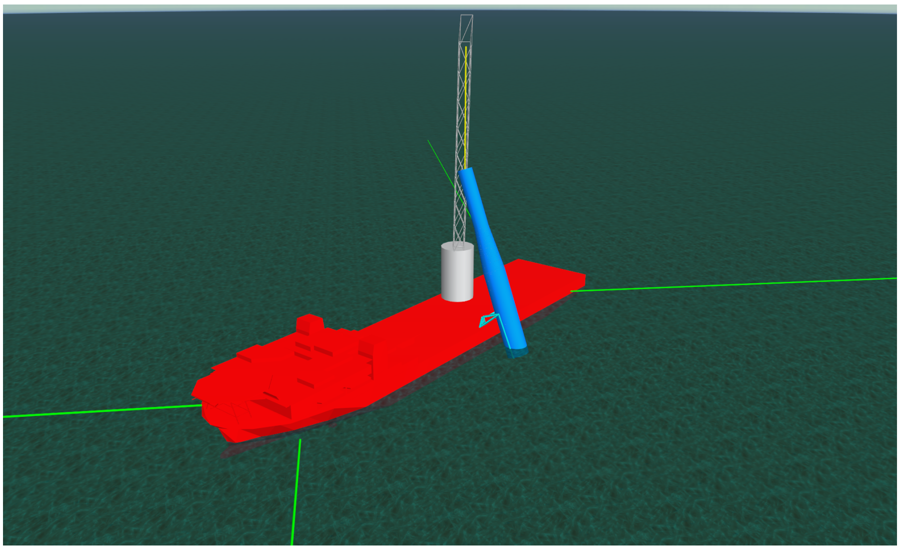

Figure 1.3: Hydrodynamic model of an upending operation

To determine the operability, the vessel and MP are subjected to a variety of sea states. Usually, the sea state consists of random waves generated from a wave spectrum that is consistent with the seas at the location of operation. A range of relevant significant wave heights, peak wave periods and wave directions is determined for the operation. Subsequently, a simulation is run for every possible combination of these parameters. For every simulation, it is determined whether the motions and forces caused by the waves are within their tolerable limits. In this manner, it can be determined in which environmental conditions the operation can safely be performed.

To be able to accurately determine the response of the vessel and MP to the waves, it is important to properly model the dynamic behaviour of the UEH as it is an important interface through which the vessel and MP interact. Conventionally, the UEH is modelled using a series of kinematic constraints that represent a stiffness. This stiffness is determined from Finite Element (FE) models. In these FE models, the UEH is subjected to a certain force. By determining the displacement caused by this force, a stiffness can be approximated in the direction of application of the force. This is done for all relevant directions and components. In this way, the stiffnesses of the kinematic constraints are determined.

The question arises, however, whether this is the ideal approach for modelling the UEH. For instance, in this approach, the mass and inertia of the UEH are neglected. Furthermore, the flexibility of the UEH is simplified as the coupling stiffnesses are neglected; a displacement in one direction does not cause a force in another direction. As upending operations become more challenging due to the MPs becoming larger, it is increasingly more important to accurately model the operations and determine their operability window. Ideally, the UEH would be modelled by implementing the existing FE models directly into the hydrodynamic simulations. However, as the models consist of thousands of nodes, this would increase the calculation times by an unreasonable ammount. Hence, TWD proposes an alternative approach. They are interested in applying Dynamic Substructuring to implement the dynamic behaviour of the UEH into the hydrodynamic model. This technique involves reducing the FE models of the

UEH in complexity by reducing the number of DoFs. This reduced model of the UEH can then be implemented into the hydrodynamic model.

1.3. Objective

To investigate the potential of using Dynamic Substructuring to model a UEH, two main questions need to be answered. The first question is the following.

> **How can Dynamic Substructuring be used to model an Upend Hinge in hydrodynamic simulations of a monopile upending operation?**

After an answer has been found to this question, the following second question needs to be answered.

> **How does the approach using Dynamic Substructuring compare to the conventional approach in terms of computation time and accuracy?**

1.4. Methodology

The methodology of this thesis is described more in detail in the subsequent chapters. Nevertheless, a summary is given here to give an overview of the entire methodology. To answer the first question, research has been done into methods for the reduction of Finite Element Method (FEM) models and their assembly into a full system. These methods are applied to a case study. This case study involves a typical upend operation. An attempt is made to reduce the FEM models of the components of the UEH that is used in this operation. Two different methods of reduction are used. Next, for each of the methods, the models of the components are assembled into a full system. Finally, both systems are implemented into the hydrodynamic simulations of the upending operation. Through the description of this process in the following chapters and the intermediate validations, the first research question can be answered.

To answer the second research question, the computation times and responses of the hydrodynamic simulations using both substructured models of the UEH are compared with the computation times and responses of the simulations using the conventionally modelled UEH. The differences are analysed and an attempt is made to explain the differences between the modelling approaches.

1.5. Thesis outline

To answer the research questions, first, all relevant theory is collected and explained in chapter 2. Next, the reduction of the models of the UEH components is discussed in chapter 3. Hereafter, the assembly of the substructures into an assembled system is addressed in chapter 4. Then, the implementation of the system and the subsequent results are discussed in chapter 5. Finally, conclusions are drawn and further research is suggested in chapter 6.

2

Theory

Throughout this thesis, a variety of mathematical and physical theory is applied. In this chapter, the relevant theory is collected and explained to maintain the cohesive narrative of the subsequent chapters. Whenever necessary, reference is made back to this chapter.

2.1. Finite Element Method (FEM)

At the foundation of the proposed approach to model the UEH lie the existing structural models of the UEH. These models are made using the Finite Element Method. The FEM is a numerical method that can be used to describe and solve complex static and dynamic mechanical systems. In this method, a structure is described as several connected elements that behave as continuous structural members. These members are known as finite elements. The idea is that by selecting proper approximate solutions in all finite elements, the solutions can be made to converge to the exact solution as the element size decreases. The connections between the elements are known as nodes. Every node can have several DoFs (Rao, 2004).

Throughout this chapter, an example model of part of a crane is used to explain concepts. The model consists of a 6-meter-long cable attached to a 15-meter-long beam and can be seen in figure 2.1a. There is a time-dependent load acting on the end of the cable. In figure 2.1b the FEM system is displayed if the beam is considered as an Euler-Bernoulli beam and the cable as an axial rod. Both the beam and the cable are divided into smaller elements connected by nodes. In the example, the elements are arbitrarily chosen to be 3 meters long. As the beam is modelled as an Euler-Bernoulli beam, each of the nodes has two DoFs while the nodes in the cable only have one DoF (Lyu, 2022).

2.2. Dynamic Substructuring

FEM modelling provides a flexible way to model complicated linear systems. However, as complexity increases, so does the required computation time. Dynamic substructuring can provide a solution to this problem. By evaluating the dynamic properties of a system componentwise, the computation time can be reduced. Furthermore, if chosen correctly, the components can be reduced through various component model reduction methods, reducing computation time even further. After being evaluated separately, the dynamic properties of the individual components can be combined to describe the full system (Klerk et al., 2008).

2.2.1. Decomposition into substructures

The first step to dynamic substructuring is splitting the system into several components or substructures. This is typically done by identifying natural boundaries within the structure

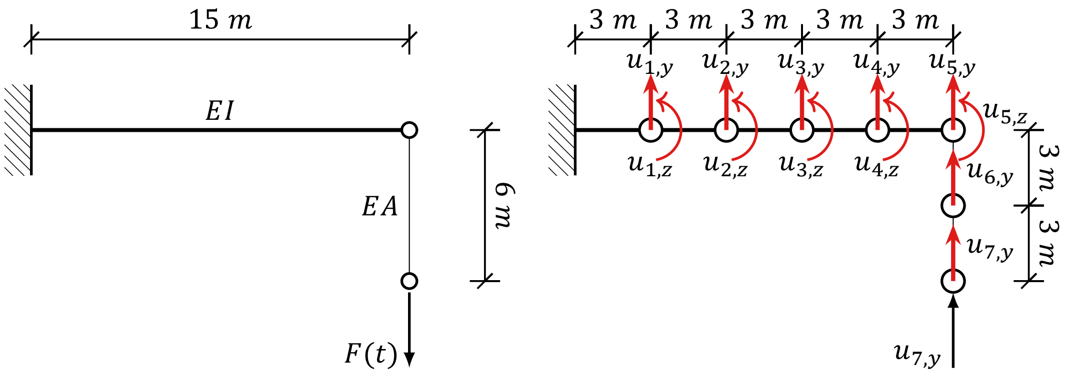

(a) Original continuous system

(b) FEM system

Figure 2.1: Finite element modelling of a crane boom and cable

where the behaviour of the structure changes. When dealing with machines consisting of several distinct parts, it often makes sense to choose these parts as substructures. As for the UEH, it has been split into the folding frame, the bucket and the U-frame; each has been modelled separately. For the example model, it makes sense to split it into the beam and the cable. These resulting subsystems can be seen in figure 2.2.

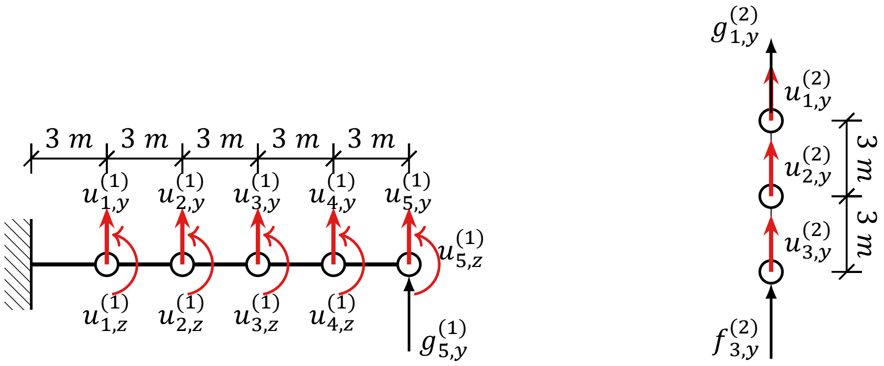

(a) FEM system for the beam

(b) FEM system cable

Figure 2.2: Substructured FEM system of a crane boom and cable

In general, the dynamics of an undamped system can be described by the following governing equation:

$$\boldsymbol{M}\ddot{\boldsymbol{u}} + \boldsymbol{K}\boldsymbol{u} = \boldsymbol{f} \tag{2.1}$$

With:

- $\boldsymbol{M}$ the Mass matrix of the system
- $\boldsymbol{K}$ the Stiffness matrix of the system
- $\boldsymbol{f}$ the external force vector, containing the external forces acting on each DoF of every node
- $\boldsymbol{u}$ and $\ddot{\boldsymbol{u}}$ the displacement and acceleration vector respectively for each DoF of every node

By dividing the structure into substructures, additional coupling forces ($\boldsymbol{g}$) are introduced in the system. These are forces, caused by one substructure acting on another substructure.

The governing equation for a substructure is thus:

$$\boldsymbol{M}^{(s)}\ddot{\boldsymbol{u}}^{(s)}+\boldsymbol{K}^{(s)}\boldsymbol{u}^{(s)}=\boldsymbol{f}^{(s)}+\boldsymbol{g}^{(s)} \tag{2.2}$$

With $\star^{(s)}$ signifying the substructure to which the matrix or vector refers. The governing equations for a full system with n substructures can be written in a block-diagonal format as:

$$\begin{bmatrix}\boldsymbol{M}^{(1)} & 0 & \cdots & 0\\ 0 & \boldsymbol{M}^{(2)} & \cdots & 0\\ \vdots & \vdots & \ddots & \vdots\\ 0 & 0 & \cdots & \boldsymbol{M}^{(n)}\end{bmatrix}\begin{bmatrix}\ddot{\boldsymbol{u}}^{(1)}\\ \ddot{\boldsymbol{u}}^{(2)}\\ \vdots\\ \ddot{\boldsymbol{u}}^{(n)}\end{bmatrix}+\begin{bmatrix}\boldsymbol{K}^{(1)} & 0 & \cdots & 0\\ 0 & \boldsymbol{K}^{(2)} & \cdots & 0\\ \vdots & \vdots & \ddots & \vdots\\ 0 & 0 & \cdots & \boldsymbol{K}^{(n)}\end{bmatrix}\begin{bmatrix}\boldsymbol{u}^{(1)}\\ \boldsymbol{u}^{(2)}\\ \vdots\\ \boldsymbol{u}^{(n)}\end{bmatrix}=\begin{bmatrix}\boldsymbol{f}^{(1)}\\ \boldsymbol{f}^{(2)}\\ \vdots\\ \boldsymbol{f}^{(n)}\end{bmatrix}+\begin{bmatrix}\boldsymbol{g}^{(1)}\\ \boldsymbol{g}^{(2)}\\ \vdots\\ \boldsymbol{g}^{(n)}\end{bmatrix} \tag{2.3}$$

Which is equivalent to:

$$\boldsymbol{M}\ddot{u}+\boldsymbol{K}\boldsymbol{u}=\boldsymbol{f}+\boldsymbol{g} \tag{2.4}$$

2.2.2. Assembly into full system

To ensure the coupling of the substructures, two conditions have to be met. Firstly, at the boundary, the DoFs of both substructures have to be compatible. This can be expressed as:

$$\boldsymbol{B}\boldsymbol{u}=\boldsymbol{0} \tag{2.5}$$

Here, $\boldsymbol{B}$ is a signed Boolean matrix if the DoFs on the boundary are matching. In the example model, only one pair of DoFs is matching. Therefore, $\boldsymbol{B}$ only consists of one row. If there was more than one pair – let's say N pairs – $\boldsymbol{B}$ would consist of N rows. This compatibility condition can also be met by reducing the total set of DoFs ($\boldsymbol{u}$) to the set of unique DoFs ($\boldsymbol{q}$). To do this, first, the nullspace of $\boldsymbol{B}$ must be computed. Then, by constructing a matrix whose columns are the vectors spanning the nullspace, the Boolean localization matrix $\boldsymbol{L}$ is found. This matrix describes the relation between $\boldsymbol{u}$ and $\boldsymbol{q}$ as follows:

$$\boldsymbol{u}=\boldsymbol{L}\boldsymbol{q} \tag{2.6}$$

The second condition to ensure the coupling of the substructures is the equilibrium condition. This refers to the force equilibrium at the boundary between two substructures. This condition can be described as:

$$\boldsymbol{L}^{T}\boldsymbol{g}=\boldsymbol{0} \tag{2.7}$$

Here $\boldsymbol{L}^{T}$ is the transpose of the localization matrix.

Application of equation 2.5, 2.6 and 2.7 to the example model gives:

$$\boldsymbol{B}\boldsymbol{u}=\begin{bmatrix}0 & 0 & 0 & 0 & 0 & 0 & 0 & 0 & 1 & 0 & -1 & 0 & 0\end{bmatrix}\begin{bmatrix}u^{(1)}_{1,y}\\ u^{(1)}_{1,z}\\ u^{(1)}_{2,y}\\ u^{(1)}_{2,z}\\ u^{(1)}_{3,y}\\ u^{(1)}_{3,z}\\ u^{(1)}_{4,y}\\ u^{(1)}_{4,z}\\ u^{(1)}_{5,y}\\ u^{(1)}_{5,z}\\ u^{(2)}_{1,y}\\ u^{(2)}_{2,y}\\ u^{(2)}_{3,y}\end{bmatrix}=u^{(1)}_{5,y}-u^{(2)}_{1,y}=0 \tag{2.8}$$

,

$$\boldsymbol{u} = \boldsymbol{Lq} = \begin{bmatrix} u_{1,y}^{(1)} \\ u_{1,z}^{(1)} \\ u_{2,y}^{(1)} \\ u_{2,z}^{(1)} \\ u_{3,y}^{(1)} \\ u_{3,z}^{(1)} \\ u_{4,y}^{(1)} \\ u_{4,z}^{(1)} \\ u_{5,y}^{(1)} = u_{1,y}^{(2)} \\ u_{5,z}^{(1)} \\ u_{1,y}^{(2)} \\ u_{2,y}^{(2)} \\ u_{3,y}^{(2)} \end{bmatrix} = \begin{bmatrix} 1 & 0 & 0 & 0 & 0 & 0 & 0 & 0 & 0 & 0 & 0 & 0 \\ 0 & 1 & 0 & 0 & 0 & 0 & 0 & 0 & 0 & 0 & 0 & 0 \\ 0 & 0 & 1 & 0 & 0 & 0 & 0 & 0 & 0 & 0 & 0 & 0 \\ 0 & 0 & 0 & 1 & 0 & 0 & 0 & 0 & 0 & 0 & 0 & 0 \\ 0 & 0 & 0 & 0 & 1 & 0 & 0 & 0 & 0 & 0 & 0 & 0 \\ 0 & 0 & 0 & 0 & 0 & 1 & 0 & 0 & 0 & 0 & 0 & 0 \\ 0 & 0 & 0 & 0 & 0 & 0 & 1 & 0 & 0 & 0 & 0 & 0 \\ 0 & 0 & 0 & 0 & 0 & 0 & 0 & 1 & 0 & 0 & 0 & 0 \\ 0 & 0 & 0 & 0 & 0 & 0 & 0 & 0 & 0 & 1 & 0 & 0 \\ 0 & 0 & 0 & 0 & 0 & 0 & 0 & 0 & 1 & 0 & 0 & 0 \\ 0 & 0 & 0 & 0 & 0 & 0 & 0 & 0 & 0 & 1 & 0 & 0 \\ 0 & 0 & 0 & 0 & 0 & 0 & 0 & 0 & 0 & 0 & 1 & 0 \\ 0 & 0 & 0 & 0 & 0 & 0 & 0 & 0 & 0 & 0 & 0 & 1 \end{bmatrix} \begin{bmatrix} u_{1,y}^{(1)} \\ u_{1,z}^{(1)} \\ u_{2,y}^{(1)} \\ u_{2,z}^{(1)} \\ u_{3,y}^{(1)} \\ u_{3,z}^{(1)} \\ u_{4,y}^{(1)} \\ u_{4,z}^{(1)} \\ u_{5,z}^{(1)} \\ u_{1,y}^{(2)} \\ u_{2,y}^{(2)} \\ u_{3,y}^{(2)} \end{bmatrix} \tag{2.9}$$

and

$$\boldsymbol{L}^T\boldsymbol{g} = \begin{bmatrix} 1 & 0 & 0 & 0 & 0 & 0 & 0 & 0 & 0 & 0 & 0 & 0 & 0 \\ 0 & 1 & 0 & 0 & 0 & 0 & 0 & 0 & 0 & 0 & 0 & 0 & 0 \\ 0 & 0 & 1 & 0 & 0 & 0 & 0 & 0 & 0 & 0 & 0 & 0 & 0 \\ 0 & 0 & 0 & 1 & 0 & 0 & 0 & 0 & 0 & 0 & 0 & 0 & 0 \\ 0 & 0 & 0 & 0 & 1 & 0 & 0 & 0 & 0 & 0 & 0 & 0 & 0 \\ 0 & 0 & 0 & 0 & 0 & 1 & 0 & 0 & 0 & 0 & 0 & 0 & 0 \\ 0 & 0 & 0 & 0 & 0 & 0 & 1 & 0 & 0 & 0 & 0 & 0 & 0 \\ 0 & 0 & 0 & 0 & 0 & 0 & 0 & 1 & 0 & 0 & 0 & 0 & 0 \\ 0 & 0 & 0 & 0 & 0 & 0 & 0 & 0 & 0 & 1 & 0 & 0 & 0 \\ 0 & 0 & 0 & 0 & 0 & 0 & 0 & 0 & 1 & 0 & 1 & 0 & 0 \\ 0 & 0 & 0 & 0 & 0 & 0 & 0 & 0 & 0 & 0 & 0 & 1 & 0 \\ 0 & 0 & 0 & 0 & 0 & 0 & 0 & 0 & 0 & 0 & 0 & 0 & 1 \end{bmatrix} \begin{bmatrix} 0 \\ 0 \\ 0 \\ 0 \\ 0 \\ 0 \\ 0 \\ 0 \\ g_{5,z}^{(1)} \\ 0 \\ g_{1,y}^{(2)} \\ 0 \\ 0 \end{bmatrix} = \begin{bmatrix} 0 \\ 0 \\ 0 \\ 0 \\ 0 \\ 0 \\ 0 \\ 0 \\ 0 \\ 0 \\ 0 \\ 0 \end{bmatrix} \tag{2.10}$$

It is now possible to combine equation 2.4, 2.6 and 2.7 as:

$$\begin{cases} \boldsymbol{ML\ddot{q}} + \boldsymbol{KLq} = \boldsymbol{f} + \boldsymbol{g} \\ \boldsymbol{L}^T\boldsymbol{g} = \boldsymbol{0} \end{cases} \tag{2.11}$$

Premultiplication of every term in the equation of motion in equation 2.11 gives the final description of the fully assembled system as:

$$\boldsymbol{\tilde{M}\ddot{q}} + \boldsymbol{\tilde{K}q} = \boldsymbol{\tilde{f}} \tag{2.12}$$

With:

$$\begin{cases} \boldsymbol{\tilde{M}} = \boldsymbol{L}^T\boldsymbol{ML} \\ \boldsymbol{\tilde{K}} = \boldsymbol{L}^T\boldsymbol{KL} \\ \boldsymbol{\tilde{f}} = \boldsymbol{L}^T\boldsymbol{f} \end{cases} \tag{2.13}$$

2.3. Component model reduction

The goal of component model reduction is to reduce the number of DoFs in the subsystem. To achieve this, the DoFs of the subsystem are described as being dependent on a smaller amount of DoFs. The new system can then be solved less expensively. Once solved, the response of the original DoFs can be determined through their relation to the reduced DoFs.

2.3.1. Guyan's reduction

The first component model reduction method to be discussed is Guyan's reduction (Guyan, 1965). To reduce the system described by equation 2.2, a distinction is made between boundary DoFs and internal DoFs. The boundary DoFs are the DoFs that are excited by coupling forces from other substructures. The internal DoFs are not. This results in the following governing system:

$$\begin{bmatrix} \boldsymbol{M}_{bb} & \boldsymbol{M}_{bi} \\ \boldsymbol{M}_{ib} & \boldsymbol{M}_{ii} \end{bmatrix} \begin{bmatrix} \ddot{\boldsymbol{u}}_b \\ \ddot{\boldsymbol{u}}_i \end{bmatrix} + \begin{bmatrix} \boldsymbol{K}_{bb} & \boldsymbol{K}_{bi} \\ \boldsymbol{K}_{ib} & \boldsymbol{K}_{ii} \end{bmatrix} \begin{bmatrix} \boldsymbol{u}_b \\ \boldsymbol{u}_i \end{bmatrix} = \begin{bmatrix} \boldsymbol{f}_b \\ \boldsymbol{f}_i \end{bmatrix} + \begin{bmatrix} \boldsymbol{g}_b \\ \boldsymbol{0} \end{bmatrix} \tag{2.14}$$

With $\star_b$ referring to the boundary DoFs and $\star_i$ referring to the internal DoFs. In this section, the superscript denoting the substructure ($\star^{(s)}$) is dropped for brevity. Note that the bottom value in the coupling force vector is zero as the internal DoFs are not excited by forces resulting from a connection with other substructures. The application of this distinction between internal and boundary DoFs on substructure (1) of the example model can be seen in figure 2.3.

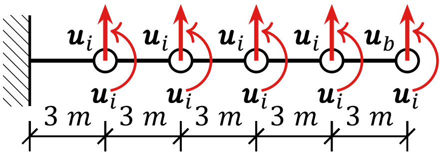

Figure 2.3: Internal and boundary DoFs of subsystem (1)

If the external forces on the internal DoFs are assumed to be zero and the internal inertia forces are neglected, the resulting system is:

$$\begin{bmatrix} \boldsymbol{K}_{bb} & \boldsymbol{K}_{bi} \\ \boldsymbol{K}_{ib} & \boldsymbol{K}_{ii} \end{bmatrix} \begin{bmatrix} \boldsymbol{u}_b \\ \boldsymbol{u}_i \end{bmatrix} = \begin{bmatrix} \boldsymbol{f}_b \\ \boldsymbol{0} \end{bmatrix} + \begin{bmatrix} \boldsymbol{g}_b \\ \boldsymbol{0} \end{bmatrix} \tag{2.15}$$

From this, the following relation between the internal and boundary DoFs can be found:

$$\boldsymbol{u}_i = \boldsymbol{S}\boldsymbol{u}_b = -\boldsymbol{K}_{ii}^{-1}\boldsymbol{K}_{ib}\boldsymbol{u}_b \tag{2.16}$$

Where $\boldsymbol{S}$ contains the static modes of the system. Hence, the number of DoFs can be reduced as follows:

$$\begin{bmatrix} \boldsymbol{u}_b \\ \boldsymbol{u}_i \end{bmatrix} = \boldsymbol{R}\boldsymbol{u}_b = \begin{bmatrix} \boldsymbol{I} \\ \boldsymbol{S} \end{bmatrix} \boldsymbol{u}_b \tag{2.17}$$

With $\boldsymbol{I}$ the identity matrix $\boldsymbol{R}$ representing the reduction matrix. The shape of a simple beam's static mode is displayed in figure 2.4.

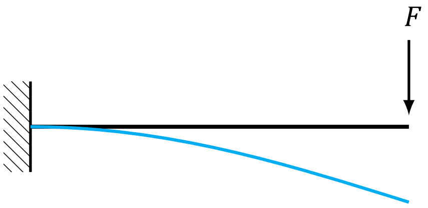

Figure 2.4: Static mode shape of a simple beam

Besides reducing the DoFs, $\boldsymbol{R}$ can also be used for reducing the mass and stiffness matrices and the external and coupling force vectors:

$$\boldsymbol{M}_m = \boldsymbol{R}^T\boldsymbol{M}\boldsymbol{R} = \boldsymbol{M}_{bb} - \boldsymbol{M}_{bi}\boldsymbol{K}_{ii}^{-1}\boldsymbol{K}_{ib} - \boldsymbol{K}_{bi}\boldsymbol{K}_{ii}^{-1}\boldsymbol{M}_{ib} + \boldsymbol{K}_{bi}\boldsymbol{K}_{ii}^{-1}\boldsymbol{M}_{ii}\boldsymbol{K}_{ii}^{-1}\boldsymbol{K}_{ib} \tag{2.18}$$

$$\boldsymbol{K}_m = \boldsymbol{R}^T\boldsymbol{K}\boldsymbol{R} = \boldsymbol{K}_{bb} - \boldsymbol{K}_{bi}\boldsymbol{K}_{ii}^{-1}\boldsymbol{K}_{ib} \tag{2.19}$$

$$\boldsymbol{f}_m = \boldsymbol{R}^T\boldsymbol{f} = \begin{bmatrix}\boldsymbol{I} & \boldsymbol{S}\end{bmatrix}\begin{bmatrix}\boldsymbol{f}_b \\ \boldsymbol{0}\end{bmatrix} = \boldsymbol{f}_b \tag{2.20}$$

$$\boldsymbol{g}_m = \boldsymbol{R}^T\boldsymbol{g} = \begin{bmatrix}\boldsymbol{I} & \boldsymbol{S}\end{bmatrix}\begin{bmatrix}\boldsymbol{g}_b \\ \boldsymbol{0}\end{bmatrix} = \boldsymbol{g}_b \tag{2.21}$$

Here, the subscript $\star_m$ indicates that the matrices are transformed to the (static) modal domain.

Premultiplying both sides of equation 2.14 with $\boldsymbol{R}^T$ and rewriting now gives the reduced system:

$$\boldsymbol{M}_m\ddot{\boldsymbol{u}}_b + \boldsymbol{K}_m\boldsymbol{u}_b = \boldsymbol{f}_m + \boldsymbol{g}_m \tag{2.22}$$

The system described in equation 2.22 is exact when applied to static problems. It is, however, an approximation when applied to dynamic problems. This is due to neglecting the internal inertia forces.

2.3.2. Craig-Bampton reduction

The second component model reduction method to be discussed is the Craig-Bampton method (Craig and Bampton, 1968). This method attempts to describe substructure motions more accurately by incorporating vibration modes. It can be seen as an extension of Guyan's method.

As eigenmodes of a dynamic system are orthogonal, the system can be described fully by a linear combination of all its modes (Rixen, 2007):

$$\boldsymbol{u} = \sum_{n=1}^{N} \eta_n \boldsymbol{\Phi}_n \tag{2.23}$$

In equation 2.23, η_n is the nth modal amplitude and $\boldsymbol{\Phi}_n$ is a matrix whose rows contain the modal shapes. Describing the system as a combination of all modes is exact as long as the system is linear. However, to reduce the system, the set of modes can be truncated as follows:

$$\boldsymbol{u} \approx \sum_{n=1}^{T} \eta_n \boldsymbol{\Phi}_n \quad T < N \tag{2.24}$$

This approximation's accuracy depends on the chosen eigenmodes and the frequency with which the system is excited.

The Guyan reduction as described in equation 2.16 can be augmented by adding several fixed-interface modes. These are the modes from the system where the boundary DoFs are constrained. The internal DoFs can then be described as:

$$\boldsymbol{u}_i = \boldsymbol{S}\boldsymbol{u}_b + \boldsymbol{\eta}\boldsymbol{\Phi} \tag{2.25}$$

where $\boldsymbol{\Phi}$ is a matrix containing the chosen interface-fixed mode shapes and $\boldsymbol{\eta}$ the corresponding modal amplitudes. The first three interface-fixed mode shapes of subsystem (1) of the example model are displayed in figure 2.5.

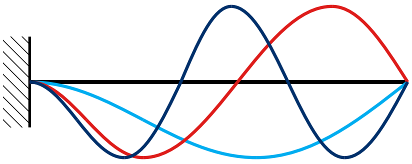

Figure 2.5: Fixed-interface mode shapes of subsystem (1)

This results in the reduction basis:

$$\begin{bmatrix} \boldsymbol{u}_b \\ \boldsymbol{u}_i \end{bmatrix} = \begin{bmatrix} \boldsymbol{u}_b \\ \boldsymbol{S}\boldsymbol{u}_b + \boldsymbol{\Phi}\boldsymbol{\eta} \end{bmatrix} = \begin{bmatrix} \boldsymbol{I} & \boldsymbol{0} \\ \boldsymbol{S} & \boldsymbol{\Phi} \end{bmatrix} \begin{bmatrix} \boldsymbol{u}_b \\ \boldsymbol{\eta} \end{bmatrix} = \boldsymbol{R} \begin{bmatrix} \boldsymbol{u}_b \\ \boldsymbol{\eta} \end{bmatrix} \tag{2.26}$$

Here $\boldsymbol{R}$ is the reduction matrix for the Craig-Bampton method. Using $\boldsymbol{R}$, the reduced mass and stiffness matrices can be constructed similarly to equations 2.18, 2.19, 2.20 and 2.21:

$$\boldsymbol{M}_m = \boldsymbol{R}^T \boldsymbol{M} \boldsymbol{R} \tag{2.27}$$

$$\boldsymbol{K}_m = \boldsymbol{R}^T \boldsymbol{K} \boldsymbol{R} \tag{2.28}$$

$$\boldsymbol{f}_m = \boldsymbol{R}^T \boldsymbol{f} \tag{2.29}$$

$$\boldsymbol{g}_m = \boldsymbol{R}^T \boldsymbol{g} \tag{2.30}$$

Equation 2.14 can now again be rewritten to:

$$\boldsymbol{M}_m \begin{bmatrix} \ddot{\boldsymbol{u}}_b \\ \ddot{\boldsymbol{\eta}} \end{bmatrix} + \boldsymbol{K}_m \begin{bmatrix} \boldsymbol{u}_b \\ \boldsymbol{\eta} \end{bmatrix} = \boldsymbol{f}_m + \boldsymbol{g}_m \tag{2.31}$$

Due to the fact that interface-fixed modes are chosen as part of the reduction basis instead of free modes, flexible substructures are not well described by the Craig-Bampton method. (Helfrich and Marchesini, n.d.) However, for the substructures described in this thesis, the Craig-Bampton method should be appropriate.

2.4. Assembly of the full reduced system

After reduction, the reduced components must be coupled into a fully assembled system. This can be done similarly as discussed in section 2.2.2. Let $\boldsymbol{\psi}$ be the vector containing the generalized DoFs (i.e. the chosen boundary DoFs and, if the Craig-Bampton method is applied, modal amplitudes) of all substructures such that:

$$\begin{bmatrix} \boldsymbol{u}^{(1)} \\ \boldsymbol{u}^{(2)} \\ \vdots \\ \boldsymbol{u}^{(n)} \end{bmatrix} = \begin{bmatrix} \boldsymbol{R}^{(1)} & 0 & \cdots & 0 \\ 0 & \boldsymbol{R}^{(2)} & \cdots & 0 \\ \vdots & \vdots & \ddots & \vdots \\ 0 & 0 & \cdots & \boldsymbol{R}^{(n)} \end{bmatrix} \begin{bmatrix} \boldsymbol{\psi}^{(1)} \\ \boldsymbol{\psi}^{(2)} \\ \vdots \\ \boldsymbol{\psi}^{(n)} \end{bmatrix} \Leftrightarrow \boldsymbol{u} = \boldsymbol{R}\boldsymbol{\psi} \tag{2.32}$$

The governing equation of the generalized system is thus:

$$\begin{bmatrix} \boldsymbol{M}_m^{(1)} & 0 & \cdots & 0 \\ 0 & \boldsymbol{M}_m^{(2)} & \cdots & 0 \\ \vdots & \vdots & \ddots & \vdots \\ 0 & 0 & \cdots & \boldsymbol{M}_m^{(n)} \end{bmatrix} \begin{bmatrix} \ddot{\boldsymbol{\psi}}^{(1)} \\ \ddot{\boldsymbol{\psi}}^{(2)} \\ \vdots \\ \ddot{\boldsymbol{\psi}}^{(n)} \end{bmatrix} + \begin{bmatrix} \boldsymbol{K}_m^{(1)} & 0 & \cdots & 0 \\ 0 & \boldsymbol{K}_m^{(2)} & \cdots & 0 \\ \vdots & \vdots & \ddots & \vdots \\ 0 & 0 & \cdots & \boldsymbol{K}_m^{(n)} \end{bmatrix} + \begin{bmatrix} \boldsymbol{\psi}^{(1)} \\ \boldsymbol{\psi}^{(2)} \\ \vdots \\ \boldsymbol{\psi}^{(n)} \end{bmatrix} = \begin{bmatrix} \boldsymbol{f}^{(1)} \\ \boldsymbol{f}^{(2)} \\ \vdots \\ \boldsymbol{f}^{(n)} \end{bmatrix} \begin{bmatrix} \boldsymbol{g}^{(1)} \\ \boldsymbol{g}^{(2)} \\ \vdots \\ \boldsymbol{g}^{(n)} \end{bmatrix} \tag{2.33}$$

$$\Leftrightarrow$$

$$\boldsymbol{M}_m \ddot{\boldsymbol{\psi}} + \boldsymbol{K}_m \boldsymbol{\psi} = \boldsymbol{f}_m + \boldsymbol{g}_m$$

Analogous to section 2.2.2, the compatibility and equilibrium conditions have to be met:

$$\begin{cases} \boldsymbol{B}_m \boldsymbol{\psi} = \boldsymbol{0} \\ \boldsymbol{L}_m^T \boldsymbol{g}_m = \boldsymbol{0} \end{cases} \tag{2.34}$$

The compatibility condition can again be met by introducing a set of unique generalized DoFs, $\boldsymbol{\xi}$. Then by premultiplying the governing equation 2.33 with $\boldsymbol{L}_m$ and noting the equilibrium condition, the system of equations of the coupled structure is found as:

$$\tilde{\boldsymbol{M}}_m\ddot{\boldsymbol{\xi}} + \tilde{\boldsymbol{K}}_m\boldsymbol{\xi} = \tilde{\boldsymbol{f}}_m \tag{2.35}$$

With:

$$\begin{cases} \tilde{\boldsymbol{M}}_m = \boldsymbol{L}_m^T\boldsymbol{M}_m\boldsymbol{L}_m \\ \tilde{\boldsymbol{K}}_m = \boldsymbol{L}_m^T\boldsymbol{K}_m\boldsymbol{L}_m \\ \tilde{\boldsymbol{f}}_m = \boldsymbol{L}_m^T\boldsymbol{f}_m \end{cases} \tag{2.36}$$

2.5. Modal analysis

To investigate the natural frequencies and corresponding modal shapes of a system, a modal analysis may be performed. This can give insight into the intrinsic dynamic properties of a system regardless of external excitation (Voormeeren, 2012) and can therefore be a good tool to validate the dynamic behaviour of a model. The natural frequencies and modal shapes can be determined for components, reduced components and even fully assembled systems, simply by solving the eigenproblem:

$$(\boldsymbol{K} - \omega_j^2\boldsymbol{M})\boldsymbol{\varphi}_j = \boldsymbol{0} \tag{2.37}$$

Here, $\boldsymbol{K}$ and $\boldsymbol{M}$ are the stiffness and mass matrix respectively. ω_j^2 refers to the natural frequency that corresponds to mode shape $\boldsymbol{\varphi}_j$.

Once the natural frequencies and mode shapes of systems are known, they can be used as a metric to determine how similar the systems behave. Of course, a simple comparison can be made between the values of the natural frequencies by looking at the relative difference. The comparison between the mode shapes is, however, less straightforward as it entails a comparison between (possibly differently scaled) vectors with multiple entries.

One elegant way to compare mode shapes is the Modal Assurance Criterion (MAC). The MAC is a statistical indicator that expresses the coherence between two modal vectors (Pastor et al., 2012). It can be calculated as follows:

$$\text{MAC}(\boldsymbol{\varphi}_a, \boldsymbol{\varphi}_b) = \frac{|\boldsymbol{\varphi}_a^T\boldsymbol{\varphi}_b|^2}{(\boldsymbol{\varphi}_a^T\boldsymbol{\varphi}_a)(\boldsymbol{\varphi}_b^T\boldsymbol{\varphi}_b)} \tag{2.38}$$

Here, $\boldsymbol{\varphi}_a$ and $\boldsymbol{\varphi}_b$ are the modal vectors to be compared. The MAC takes a value between 0 and 1. A value of 1 indicates that the modal vectors have the same shape. A value of 0.9 or higher indicates a close resemblance between the modes. The closer the MAC value is to zero, the less resemblance there is between the modes.

By computing the MAC for all modes of two systems, an overview can be made of which modes correspond to one another. An example of such an overview is given in figure 2.6. A MAC plot gives insight into how similar the dynamic properties of two systems are. When comparing a model to a reduction or simplification of that model, it can also convey information on which modes are captured well by the simpler model. This may be valuable when certain modes of a system are irrelevant. This may be the case when one is only interested in global modes and not in local modes. Also, when a system is only subjected to forcings in a certain frequency range, only the mode corresponding to natural frequencies in that range may be of interest. Hence, a MAC plot can be a great tool to compare a reduced or simplified model to its original.

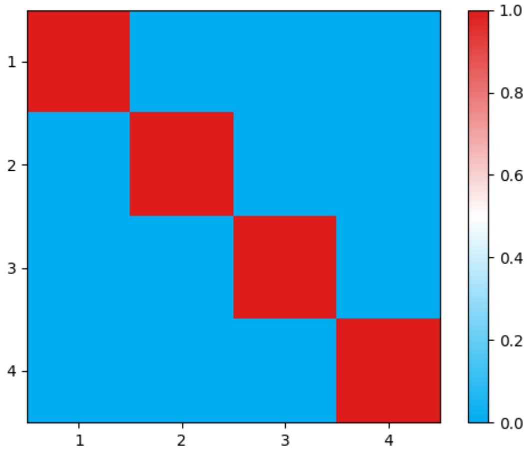

Figure 2.6: Example of a MAC plot for two systems with the same modal vectors

2.6. Proper Orthogonal Decomposition

To investigate the characteristics of a system in the time domain, a Proper Orthogonal Decomposition (POD) can be used. A POD is a method for obtaining low-dimensional approximate descriptions of a high-dimensional matrix (Liang et al., 2002). It can be applied to a time-varying signal to capture the dominant components of that signal, so-called Proper Othogonal Modes (POMs).

The method can be applied in multiple ways such as by constructing a sample covariance matrix and by using the Singular Value Decomposition (SVD) (Voormeeren, 2012). In this section, the method using the SVD will be detailed as this is the method that is applied in this thesis. Suppose that a time-varying signal is obtained and that m snapshots of this signal are collected in a response matrix $\boldsymbol{Z}$ as follows:

$$\boldsymbol{Z} = \begin{bmatrix} \boldsymbol{u}_1 & \dots & \boldsymbol{u}_m \end{bmatrix} \tag{2.39}$$

Here $\boldsymbol{u}_i$ is the displacement vector at snapshot i.

Then, the mean-centred response matrix $\boldsymbol{X}$ is found as:

$$\boldsymbol{X} = \begin{bmatrix} \boldsymbol{u}_1 - \boldsymbol{\mu} & \dots & \boldsymbol{u}_m - \boldsymbol{\mu} \end{bmatrix} \tag{2.40}$$

Here $\boldsymbol{\mu}$ is a vector containing each of the time averages of the DoFs in the displacement vector.

Next, the SVD of the mean-centred response matrix $\boldsymbol{X}$ is found as:

$$\boldsymbol{X} = \boldsymbol{U}\boldsymbol{\Sigma}\boldsymbol{V}^T \tag{2.41}$$

With $\boldsymbol{U}$ the matrix of left singular vectors, $\boldsymbol{\Sigma}$, the pseudo-diagonal matrix containing the singular values and $\boldsymbol{V}$ the matrix of right singular vectors.

Each of these matrices provides a specific type of information about the time-varying signal. The columns of matrix $\boldsymbol{U}$ contain the POMs. These vectors form the basis that captures the spatial behaviour of $\boldsymbol{X}$. The singular values in $\boldsymbol{\Sigma}$ are equal to the Proper Orthogonal Values (POVs) of matrix $\boldsymbol{X}$. They are ordered in $\boldsymbol{\Sigma}$ from greatest to least and they provide information on the relative energy content of the contained in the associated POM. The columns of matrix $\boldsymbol{V}$ contain the time modulation of the corresponding POMs.

By decomposing the response into its spatial and temporal behaviour, responses can be better compared. As small differences in temporal behaviour (e.g. slightly different frequencies), cause time signals to drift apart over time, it can be very useful to focus only on the temporal behaviour. Furthermore, it can be shown that the POMs form a basis that captures the most energy per mode as possible. As the POVs (and therefore the POMs) are ordered, the response can usually be accurately described by only the first handful of modes.

2.6.1. Poper Orthogonal Modal Assurance Criterion

The concept of the MAC can also be applied to POMs. In this way, the responses of systems can be compared with one another. In this thesis, such a comparison is referred to as a Proper Orthogonal Modal Assurance Criterion (POMAC).

The computation of a POMAC is very similar to the computation of a MAC and is done as follows:

$$\text{POMAC}(\mathbf{POM}_a, \mathbf{POM}_b) = \frac{|\mathbf{POM}_a^T \mathbf{POM}_b|^2}{(\mathbf{POM}_a^T \mathbf{POM}_a)(\mathbf{POM}_b^T \mathbf{POM}_b)} \tag{2.42}$$

Here, $\mathbf{POM}_a$ and $\mathbf{POM}_b$ are the proper orthogonal modes to be compared. Similar to the MAC, the POMAC takes a value between 0 and 1.

3

Component reduction

One of the goals of this thesis is to arrive at a reduced model of a monopile upending hinge while retaining adequate accuracy. To this end, TWD has provided FE models of the components of a UEH that they have designed in the past. In this chapter, the reduction of these models is discussed.

In section 3.1, the models that were provided are discussed in a general sense. In section 3.2, the reduction of each of the components is explained. The reduced models are also compared with the original models. In section 3.3, the reduction process is evaluated.

3.1. Provided models

The specifics of the UEH that is modelled are not of great importance for the main goals of this thesis. The focus lies on the reduction of the model, with the design of the UEH being considered a given. It is nevertheless valuable to discuss briefly the models that form the starting point of the reduction and modelling process.

3.1.1. Original models

The models provided by TWD are of a UEH that was designed for one of their clients. The UEH is designed to be used on a vessel in floating conditions. It can be folded into several configurations to improve clearance during transit and facilitate the positioning of the MP into the UEH. It can also be adjusted to be suited for a variety of pile lengths. It is to be noted, however, that for the model, only the configuration to be used during the upending procedure is relevant as only this procedure is modelled in this thesis. This configuration of the UEH is displayed in figure 3.1.

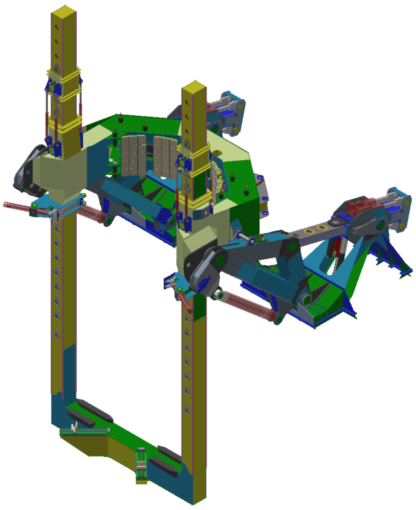
Figure 3.1: Upend hinge in upending configuration

The UEH designed by TWD consists of six main components:

- Two folding frames that are identical but mirrored
- One bucket

- One U-frame
- Two identical back braces

For each of these components, TWD has created a detailed FEM model. For more information about FEM modelling, please refer to section 2.1. As the two folding frames are identical but mirrored copies of one another, they share a model. For this same reason, the back braces also share a model. The models are displayed in figure 3.2.

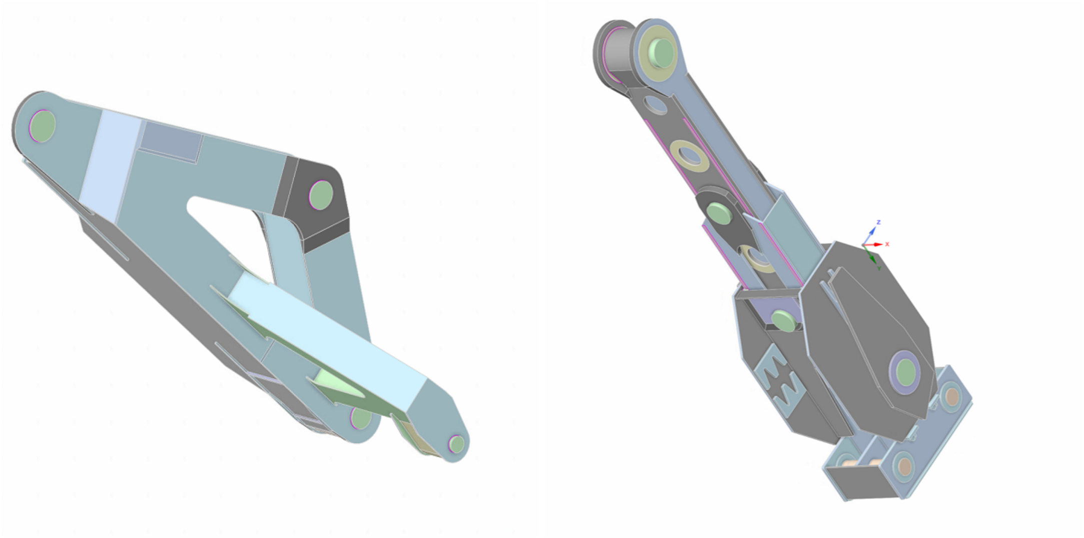

(a) Folding frame (b) Back brace

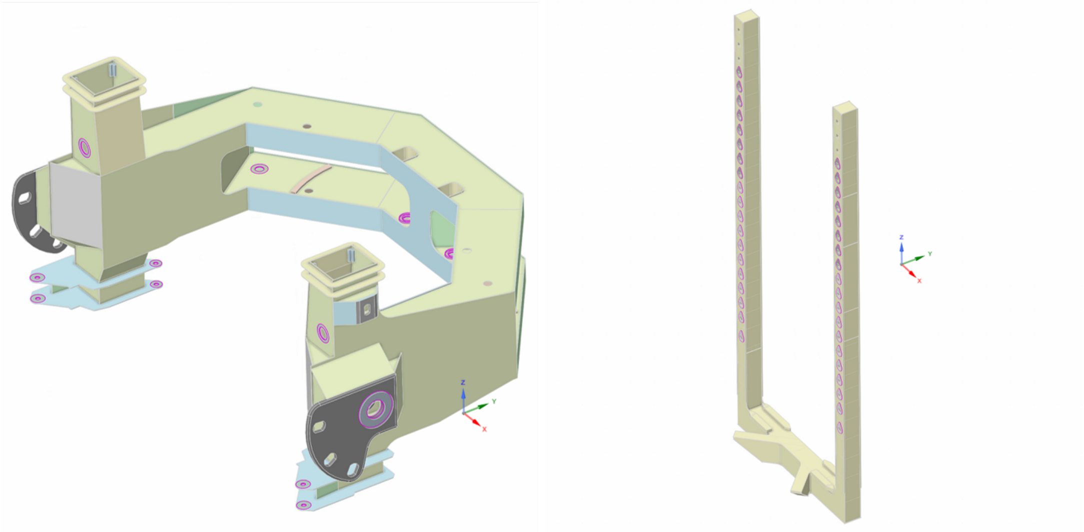

(c) Bucket (d) U-frame

Figure 3.2: Original FEM models of the components of the UEH

TWD created the models to determine and check the structural strength of the components. Because of this, to be able to investigate local peak stresses, the models are extremely detailed. The models vary from consisting of 140 000 - 630 000 Nodes or 420 000 - 1 890 000 DoFs. For the determination of global behaviour, this is an excessive amount of detail.

3.1.2. Simplified models

To achieve the reduced models, the mass and stiffness matrix need to be reduced. The computation time that is required for this reduction is related to the matrix dimension to the power of 2 to 3 (Li et al., 2020). In order to improve calculation times it is therefore decided to use simplified FEM models as the basis of the final model. These simplified models were made specifically to be used as the basis for the reduction. Usually, however, during the design process, sufficiently simple models are made to determine the global behaviour of the system. In these cases, the simplified models do not need to be made specifically for the reduction process.

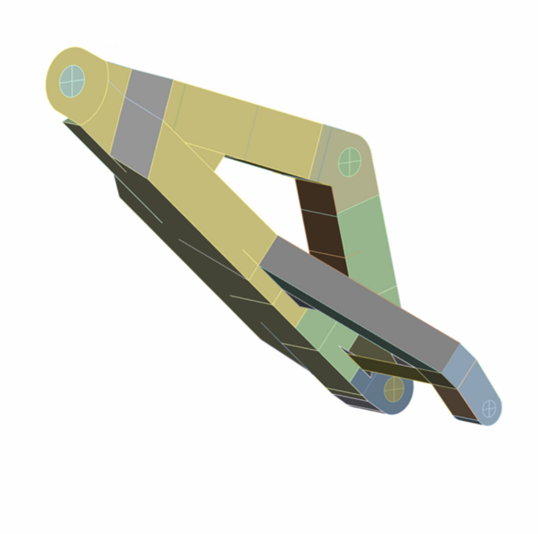

(a) Folding frame

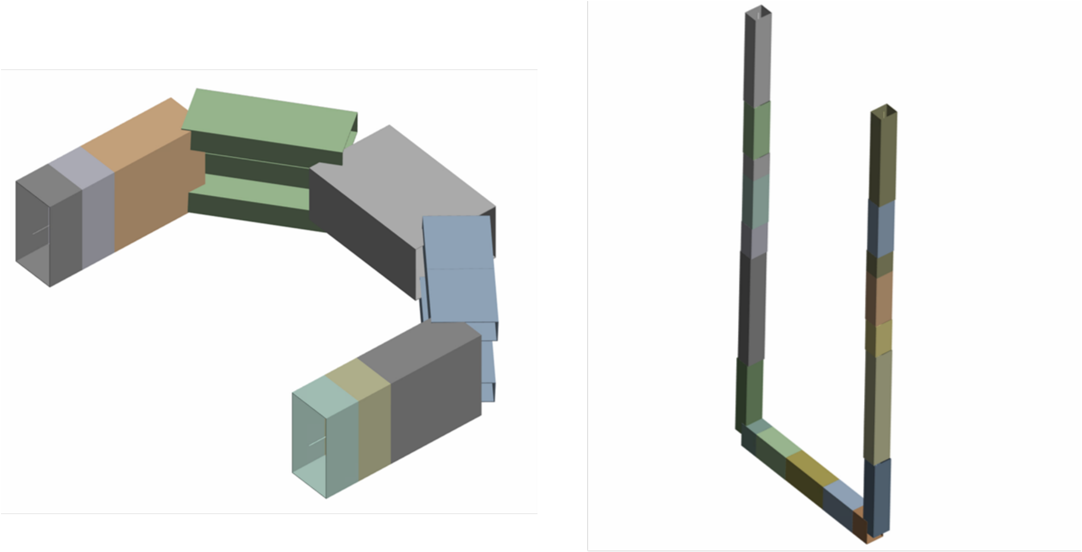

(b) Bucket

(c) U-frame

Figure 3.3: Simplified FEM models of the components of the UEH

The original models are made up of 3D elements. The simplified model of the folding frames is made up of 2D shell elements. This choice was made because the folding frames are made entirely from plate steel. 2D shell elements, therefore, are a good representation of reality (“Mechanical APDL 2023 R1 Element Reference”, 2023). The simplified models of the bucket and U-frame are made up of 1D beam elements. This is because they consist of sections with near-constant cross-sections. The back brace model is not simplified because this component is not reduced. Due to the simplicity of the function of the back brace during upending (it is a rigid bar), the back brace will be dealt with differently from the other components. This is further explained in section 3.2.4. The three simplified models are displayed in figure 3.3.

3.1.3. Comparison of FEM models

By both applying 1D and 2D instead of 3D fem and removing flanges and other parts that are irrelevant for the global mass and stiffness of the components, a great reduction in the amount of DoFs is achieved. This can be seen in table 3.1.

Table 3.1: Comparison of the number of DoFs in the original and the simplified models

	No. DoFs Original model	**No. DoFs Simplified model**
Folding frame	800685	12930
Bucket	415950	498
U-frame	1895847	642

To validate the simplified models a modal analysis of both the original and the simplified models is performed. More information about modal analyses can be found in section 2.5. The MAC plots can be found in Appendix A. An overview of the comparison of the matched modes is displayed in tables 3.2, 3.3 and 3.4.

Table 3.2: Comparison of matched modes of original and simplified Folding frame model

Natural frequency Original model (Hz)	**Natural frequency Simplified model (Hz)**	**Natural frequency error (%)**	**MAC**
25.34	26.82	5.87	0.99
36.35	33.06	9.05	0.94
47.95	47.15	1.68	0.96
50.82	50.89	0.14	0.97
54.67	57.73	5.61	0.65
59.29	48.60	18.02	0.94
59.60	60.05	0.76	0.64

Table 3.3: Comparison of matched modes of original and simplified Bucket Model

Natural frequency Original model (Hz)	**Natural frequency Simplified model (Hz)**	**Natural frequency error (%)**	**MAC**
5.63	6.82	21.21	0.98
7.80	7.28	6.71	0.85
14.74	13.30	9.77	0.69
15.75	15.89	0.89	0.96
20.57	24.38	18.48	0.73
23.49	13.30	43.38	0.87
33.89	37.10	9.47	0.94

It can be seen that in general, the original and simplified models have comparable natural frequencies and corresponding mode shapes. There are, however, several noteworthy differences.

Table 3.4: Comparison of matched modes of original and simplified U-frame Model

Natural frequency Original model (Hz)	**Natural frequency Simplified model (Hz)**	**Natural frequency error (%)**	**MAC**
0.79	0.85	8.03	1.00
1.11	1.30	17.30	0.99
2.19	2.38	8.97	1.00
4.64	5.05	8.86	0.99
4.91	5.28	7.62	0.99
6.07	6.76	11.44	0.94
6.16	6.95	12.92	0.98

Firstly, several modes have MAC values below 0.9, indicating a poor match in mode shape. However, these badly matching mode shapes correspond to natural frequencies above 10 Hz. The UEH is designed for conditions at sea where most of the wave energy is associated with waves of frequencies between 0.05 and 0.2 Hz (Falnes, 2002). Therefore, the modes with relatively high natural frequencies are deemed to be of less significance.

Secondly, the natural frequency for several lower-frequency modes is higher in the simplified models than in the original modes. The difference is higher than expected. An attempt was made to reduce this difference between the models. This was, however, unsuccessful. There are several possible reasons for the difference between the models, for instance:

- The simplified models are 1D or 2D as opposed to the original 3D models. This reduction in dimensions may have, inadvertently, constrained the simplified models. This may have increased the stiffness of the model and therefore increased the natural frequency.
- Several flanges and other parts of the original models were omitted from the simplified models. Even though an attempt was made to represent the mass of these parts in the simplified model, this may not have been entirely successful. A reduction in mass results in a higher natural frequency.

The differences between the original model and the simplified models are greater than expected. Nevertheless, the simplified models form the basis of the subsequent model reduction. This is because an initial investigation into the cause of the differences was fruitless. A more in-depth investigation into the simplification of FEM models is deemed to be outside of the scope of this thesis. As mentioned at the beginning of this section, the focus is not on the specific model to which the reduction is applied but rather on the reduction procedure itself.

3.2. Reduction and validation of models

In order to reduce the models, first, boundary nodes have to be selected. This selection is made such that at every point where the component is connected to another component, the vessel or the monopile, at least one boundary node exists. Hereafter, both the Guyan and the Craig-Bampton reduction can be applied. For more information on these reduction methods please refer to section 2.3.

For the Craig-Bampton reduction, the first five interface-fixed modes are chosen to be added to the Guyan reduction. The interface-fixed modes have high frequencies compared to prevalent wave frequencies so the inclusion of five modes may seem excessive. However, by including the first five modes, any difference in response of the system caused by this inclusion will be evident when comparing the response to that of the Guyan-reduced system. If there is a negligible difference between the responses, it can be asserted with confidence that the Guyan-reduced system is adequate. If there is a bigger difference, further investigation can be done into which modes contribute to this difference.

Once the reduced models are made, they are compared with the model on which they are based. Similarly to the comparison between the original and the simplified models, this is done by modal analysis.

3.2.1. Folding frame

For the folding frame, the boundary nodes are chosen at the centre of each of its holes. These are the locations where the frame interfaces with other components or with the vessel. Figure 3.4 gives an overview of the nodes. In total, seven boundary nodes are chosen. As each boundary node has six DoFs, this results in 42 boundary DoFs. As for the Craig-Bampton, 5 modes shapes are added, and thus the Craig-Bampton reduced system consists of 47 DoFs.

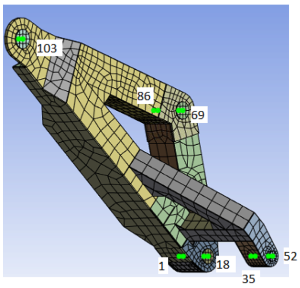

Figure 3.4: Overview of boundary nodes for Folding frame model (the numbers refer to the node numbers assigned by the FEM software)

The folding frame is reduced both with a Guyan and with a Craig-Bampton reduction. An overview of the modal comparison between the reduced and the unreduced models can be seen in figure 3.5 and table 3.5. It can be seen that the Craig-Bampton reduction matches better than the Guyan reduction with the unreduced model. This is to be expected as the Craig-Bampton reduction is an extension of the Guyan reduction and should therefore match better. Furthermore, for both reductions, the modes with lower frequencies match up better. The higher frequency modes have lower MAC values and higher errors in natural frequency. This is more so the case for the Guyan reduction than for the Craig-Bampton reduction.

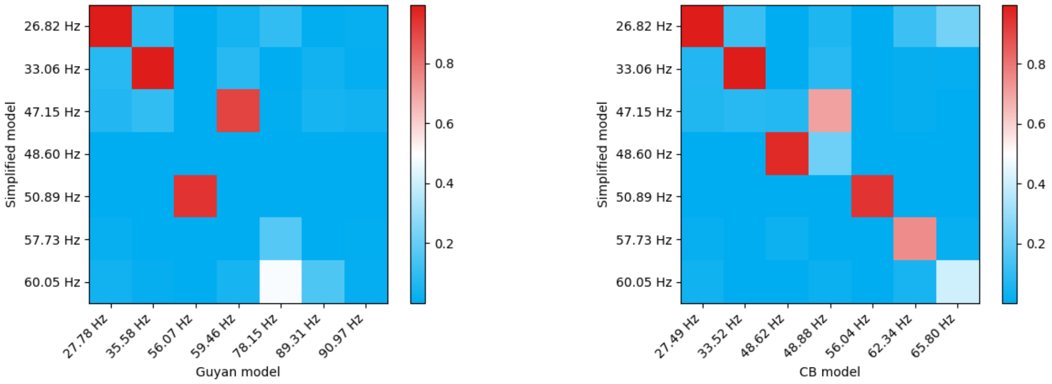

(a) Simplified model - Guyan model

(b) Simplified model - Craig-Bampton model

Figure 3.5: MAC plots for Folding frame model. Note: the modes are ordered by natural frequency. As the natural frequencies do not perfectly match between the models neither does the ordering of the modes. This results in some mode pairs appearing off the main diagonal.

Table 3.5: Comparison of matched modes of simplified model and Guyan and Craig-Bampton reduced models of Folding frame

	Guyan			**Craig-Bampton**		
Natural frequency Simplified (Hz)	**Natural frequency (Hz)**	**Nat. freq. error (%)**	**MAC**	**Natural frequency (Hz)**	**Nat. freq. error (%)**	**MAC**
26.82	27.78	3.56	0.99	27.49	2.50	1.00
33.06	35.58	7.64	0.99	33.52	1.41	0.99
47.15	59.46	26.13	0.91	48.88	3.69	0.70
48.60	59.46	22.35	0.00	48.62	0.04	0.96
50.89	56.07	10.18	0.94	56.04	10.12	0.94
57.73	78.15	35.36	0.17	62.34	7.98	0.75
60.05	78.15	30.13	0.48	65.80	9.57	0.40

3.2.2. Bucket

For the bucket, the boundary nodes are chosen at the places where it connects to the folding frame and U-frame, and where it supports the MP. An overview of these nodes is displayed in figure 3.6. It is important to note that even though multiple dots are displayed across each cross-section, they represent only one node. This is due to the 1D nature of this mode. Hence, there are four boundary nodes. As each boundary node has six DoFs, this results in 24 boundary DoFs. As for the Craig-Bampton, 5 modes shapes are added, and thus the Craig-Bampton reduced system consists of 29 DoFs.

The model of the bucket is also reduced through a Guyan and a Craig-Bampton reduction. In figure 3.7 and table 3.6 the reduced systems are again compared to their unreduced counterpart. The Craig-Bampton reduced model matches marginally better than the Guyan reduction. Again, the modes with lower frequencies match closer than the modes with higher frequencies. Overall though, it is apparent that the modal properties of the Guyan and the Craig-Bampton reduction both are very similar to those of the unreduced system.

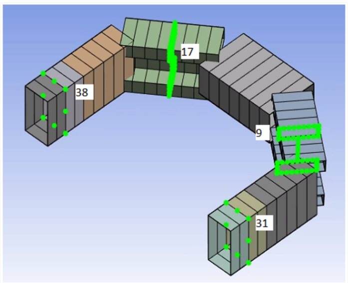

Figure 3.6: Overview of boundary nodes for Bucket model

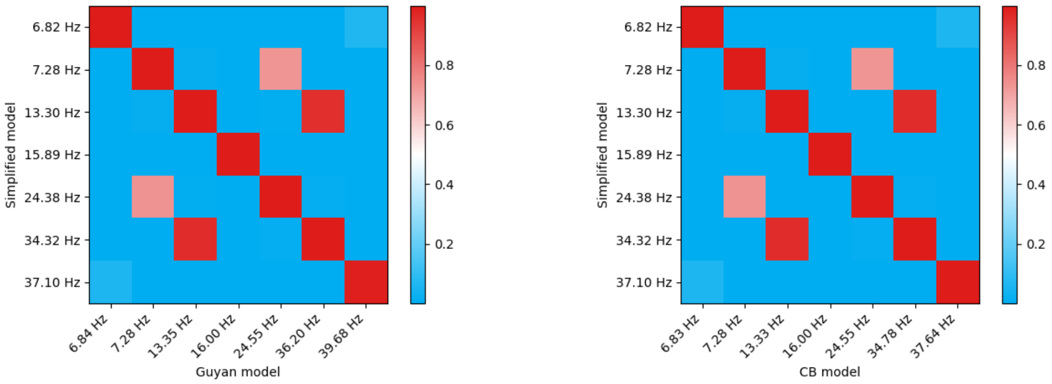

(a) Simplified model - Guyan model

(b) Simplified model - Craig-Bampton model

Figure 3.7: MAC plots for Bucket model

Table 3.6: Comparison of matched modes of simplified model and Guyan and Craig-Bampton reduced models of Bucket

	Guyan			**Craig-Bampton**		
Natural frequency Simplified (Hz)	**Natural frequency (Hz)**	**Nat. freq. error (%)**	**MAC**	**Natural frequency (Hz)**	**Nat. freq. error (%)**	**MAC**
6.82	6.84	0.26	1.00	6.83	0.13	1.00
7.28	7.28	0.09	1.00	7.28	0.09	1.00
13.30	13.35	0.41	1.00	13.33	0.27	1.00
15.89	16.00	0.70	1.00	16.00	0.70	1.00
24.38	24.55	0.72	1.00	24.55	0.70	1.00
34.32	36.20	5.49	0.99	34.78	1.34	1.00
37.10	39.68	6.95	0.99	37.64	1.46	1.00

3.2.3. U-frame

The boundary nodes of the U-frame are chosen at the places where it connects to the folding frame and bucket, and where it supports the MP. The boundary nodes are displayed in figure 3.8. As is the case with the bucket, each set of dots across a cross-section represents one node. As can be seen, four boundary nodes are chosen for the U-frame. As each boundary node has six DoFs, this results in 24 boundary DoFs. As for the Craig-Bampton, 5 modes shapes are added, and thus the Craig-Bampton reduced system consists of 29 DoFs.

Like the previous two models, the model of the U-frame is reduced with a Guyan and a Craig-Bampton reduction. The comparison of the reduced systems with the unreduced system is shown in figure 3.9 and table 3.7. This comparison is very similar to the comparison of the bucket models. Again the Craig-Bampton reduced model matches slightly better than the Guyan reduced model. The modes with a higher frequency are also in this case less concordant than the modes with a lower frequency. Once more, it is, however, clear that the modes match closely to the

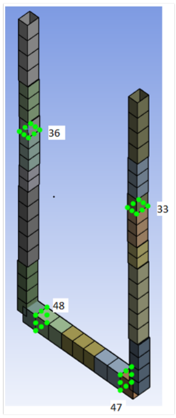

Figure 3.8: Overview of boundary nodes for U-frame model

unreduced models for both the Guyan and the Craig-Bampton reduced models.

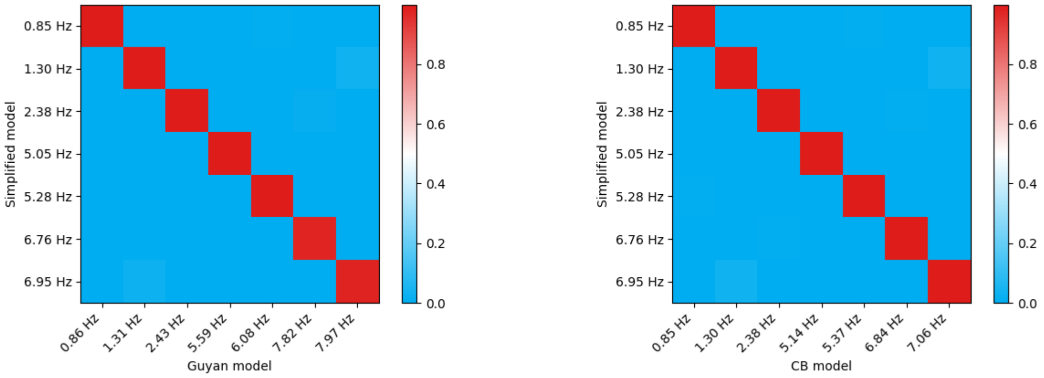

(a) Simplified model - Guyan model

(b) Simplified model - Craig-Bampton model

Figure 3.9: MAC plots for U-frame model

Table 3.7: Comparison of matched modes of simplified model and Guyan and Craig-Bampton reduced models of U-frame

	Guyan			**Craig-Bampton**		
Natural frequency Simplified (Hz)	**Natural frequency (Hz)**	**Nat. freq. error (%)**	**MAC**	**Natural frequency (Hz)**	**Nat. freq. error (%)**	**MAC**
0.85	0.86	0.58	1.00	0.85	0.01	1.00
1.30	1.31	0.86	1.00	1.30	0.05	1.00
2.38	2.43	1.86	1.00	2.38	0.10	1.00
5.05	5.59	10.61	0.99	5.14	1.78	1.00
5.28	6.08	15.09	0.99	5.37	1.75	1.00
6.76	7.82	15.62	0.98	6.84	1.17	1.00
6.95	7.97	14.68	0.98	7.06	1.54	1.00

3.2.4. Back brace

As mentioned before, the back braces act as a rigid bar during upending. Because they are connected to the vessel and the folding frames with hinges they can be considered to be two-force members. They are therefore modelled as simple springs. The stiffness of these springs was determined using the FEM model. When subjected to a tensile force of 10 000 kN, the back brace deforms by 2.58 mm. From this, the equivalent spring stiffness is determined to be:

$$k = \frac{F}{u} = \frac{1 \times 10^7}{2.58 \times 10^{-3}} = 3.88 \times 10^9 \mathrm{N/m} \tag{3.1}$$

Hence, both back braces will be modelled as springs with a linear spring stiffness of 3.88×10^9 N/m.

3.3. Conclusions of the reduction process

The first step of the reduction process is the simplification step from the supplied original models to the simplified models as described in section 3.1. From the comparison between the natural frequencies and mode shapes of the original models and the simplified models, it is clear that the simplified models do not match the original models as well as desired. The difference between the models is too large. Nevertheless, the simplified models form the basis of the subsequent reductions. The disparity is deemed to be a point for further research but it is out of the scope of this thesis to investigate further.

The second step of the reduction process is the actual reduction of the simplified models. For all models, a significant reduction in DoFs is achieved as can be seen in table 3.8.

Table 3.8: Comparison of the number of DoFs in the simplified and the reduced models

	Number of DoFs		
	Simplified model	**Guyan model**	**Craig-Bampton model**
Folding frame	12930	42	47
Bucket	498	24	29
U-frame	642	24	29

The reduction is greatest for the model of the folding frames. This is also reflected in a sense by the accuracy of the reductions of this model. Even though the accuracy is deemed satisfactory, it is worst for reductions of the folding frames model. Another reason for the relatively limited accuracy of this model is the fact that the folding frame is quite stiff; its eigenfrequencies are relatively high. As can be seen for all models, modes with higher eigenfrequencies are worse described by the reductions. Nevertheless, the first 2 modes of the reduction of the folding frame match well even though they have a natural frequency upwards of 25 Hz. As the UEH is designed for forcings with significantly lower frequencies, both reductions are deemed to be sufficiently accurate.

The reduction of the bucket and U-frame models is less substantial. The accuracy, however, is significantly higher. When looking at the comparisons between the natural frequencies and modal shapes, it is apparent that the reductions still describe the original dynamic characteristics well. This holds for both the Guyan and the Craig-Bampton reductions

From the validation of the models, it seems that even though the Craig-Bampton reductions describe the dynamic properties better, the Guyan reductions describe them well enough as well. As both reductions show promise, it is decided to move forward with the assembly of two reduced systems. One where the substructures are Guyan reduced and one where the substructures are Craig-Bampton reduced with 5 interface-fixed modes. After the assembly, it can be evaluated whether the Craig-Bampton reduction is superfluous.

4

System Assembly

In chapter 3 the models of the components of the UEH have been reduced. The next step is to combine the reduced models into a fully assembled system. In this chapter, the assembly and validation of the UEH model is illustrated.

This chapter is structured as follows. In section 4.1, it is explained how the substructures are coupled into an assembled system. In section 4.2 the assembled systems are compared with one another in the modal domain. In section 4.3, the reduced systems are compared in time domain.

4.1. Coupling

To assist the discussion of the coupling of the substructures, the boundary nodes are named as shown in figure 4.1. The names relate to the models to which they belong:

- FF: Folding Frame
- BUC: Bucket
- FFM: Folding Frame Mirrored
- UF: U-Frame

The coupling of the substructures is done for the unreduced system, as described in subsection 2.2.2. The coupling for the reduced systems is achieved as described in section 2.4. For all systems, the same DoFs of the same nodes are coupled. An overview of which DoFs are coupled is given in table 4.1. Here, the first 2 columns specify which nodes are coupled. the right-most column specifies which DoFs of these nodes are coupled. As mentioned before, each node has six DoFs: three translational and three rotational. The translation in the x, y and z direction are named X, Y and Z respectively. The rotations around the x, y and z axis are named RX, RY and RZ respectively. The chosen axis system is shown in figure 4.1.

Table 4.1: Overview of which DoFs of which nodes are coupled

Coupled Nodes		**Coupled DoFs**
FF1	BUC1	X, Y, Z, RY, RZ
FFM1	BUC4	X, Y, Z, RY, RZ
UF1	BUC1	X, Y, Z, RX, RY, RZ
UF4	BUC4	X, Y, Z, RX, RY, RZ

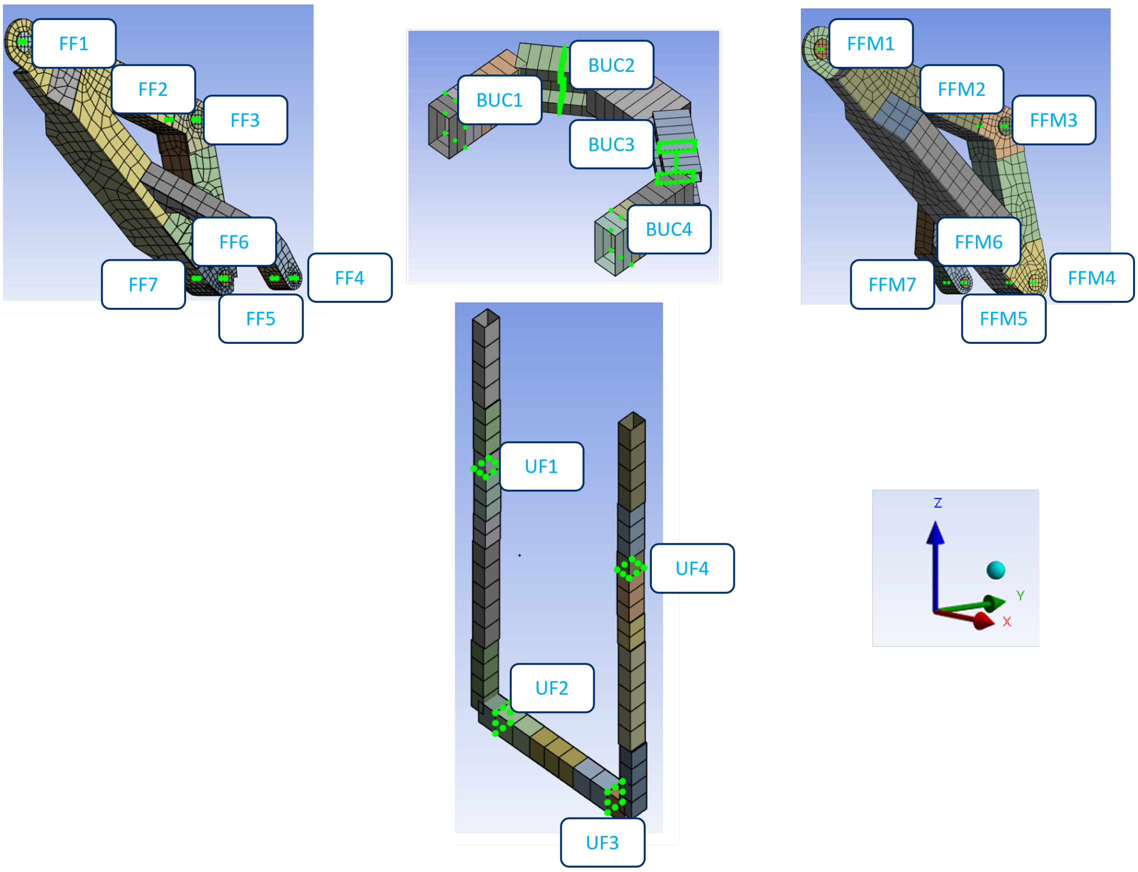

Figure 4.1: Overview of boundary node naming and the chosen coordinate system

As can be seen in table 4.1, the U-frame and the bucket are coupled rigidly. The coupling of the folding frames and the bucket allows for rotation around the x-axis. This is, of course, to allow for the main function of the UEH: *hinging*.

One thing to note is that the coupling of DoFs means their displacements are equal, not necessarily their locations. This is done due to the simplified nature of the models. In reality, pins and other components connect the substructures. In the simplification, these were omitted. Therefore, small gaps exist between the substructures.

4.2. Validation in modal domain

Similarly to the individual components, the assembled systems are compared in the modal domain. The assembled systems, however, are not compared by their free modes. They are compared by their modes with the folding frames fixed to the deck by boundary nodes FF2-7 and FFM2-7. Furthermore, a MP with a mass of 2750 tonnes is modelled to be attached to the U-frame. This is done, simply by altering the U-frame's mass matrix. This alteration was made to compare the systems in a realistic setting; this is also a configuration when the UEH is in use. The comparison is shown in figure 4.2 and table 4.2.

From this comparison, it becomes apparent that both the Guyan reduced and the Craig-Bampton reduced match very well. As seen before, the Craig-Bampton has slightly lower errors in natural frequency and higher MAC values.

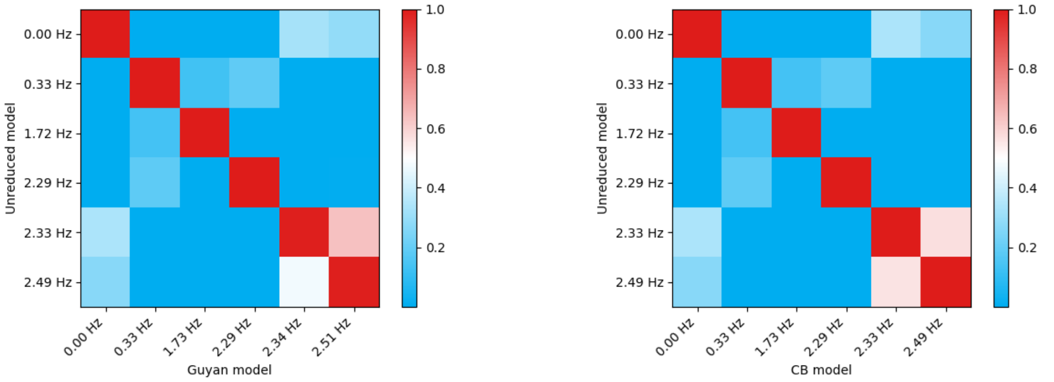

(a) Unreduced system - Guyan reduced system

(b) Unreduced system - Craig-Bampton reduced system

Figure 4.2: MAC plots for assembled systems

Table 4.2: Comparison of matched modes of unreduced assembled system and Guyan and Craig-Bampton reduced assembled systems

	Guyan			**Craig-Bampton**		
Natural frequency Unreduced (Hz)	**Natural frequency (Hz)**	**Nat. freq. error (%)**	**MAC**	**Natural frequency (Hz)**	**Nat. freq. error (%)**	**MAC**
0.00	0.00	0.00	1.00	0.00	0.00	1.00
0.33	0.33	0.00	1.00	0.33	0.00	1.00
1.72	1.73	0.33	1.00	1.73	0.10	1.00
2.29	2.29	0.23	1.00	2.29	0.01	1.00
2.33	2.34	0.54	0.99	2.33	0.04	1.00
2.49	2.51	1.00	0.99	2.49	0.04	1.00

4.3. Validation in time domain

To further validate the fully assembled model, a simple simulation in the time domain is performed. A ship is modelled that undergoes six types of motion: surge, sway, heave, roll, pitch and yaw. These six motions are harmonic in nature and are defined in the Centre of Gravity (CoG). They have varying amplitudes and phases but they share the same period. This is to model a very simple sea state.

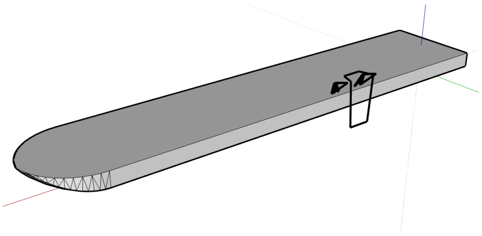

Figure 4.3: Conceptual sketch of the system that is simulated for the validation in time domain

The UEH is fixed to the ship as seen in figure 4.3. This means nodes FF2-7 and FFM2-7 move with the motions of the ship. The other DoFs of the system are unconstrained. In this simulation, gravity is not present.

The simulation is performed with an initial value solver for Ordinary Differential Equation (ODE) systems. More specifically, the *solve_ivp()* function is used from the *Python* package

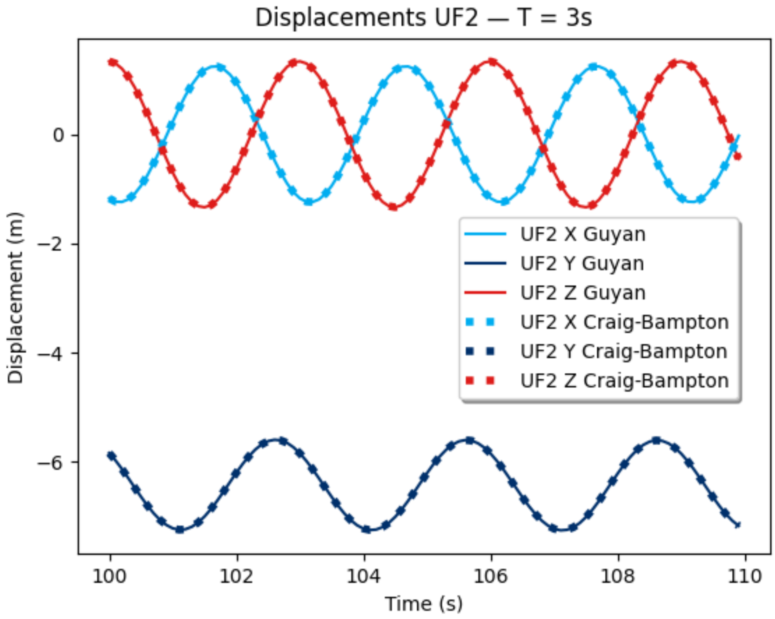

Figure 4.4: A comparison of displacement over time for the Guyan and the Craig-Bampton reduced systems with a forcing period of 3s. Note that as no gravity is present in the simulation, the hinge begins to tilt slightly as can be seen by the shifted mean of the Y displacement.

SciPy. The unreduced system consists of too many DoFs to be simulated this way. This makes sense as the reason for the reduction process is to reduce the system so that it *can* be used in a dynamic simulation. Nevertheless, it prevents the comparison of the response of the unreduced and reduced systems in the time domain. The motions of the reduced systems can only be compared against one another.

The first comparison is qualitative. In figure 4.4 the time trace of the displacements of node UF2 is plotted for an arbitrary time frame for both the Guyan and the Craig-Bampton reduced system. The time traces are indistinguishable from each other, which points to an accurate description of the motion.

To quantitate the comparison of the simulations, the technique of Proper Orthogonal Decomposition (POD) is applied to the responses of the simulations. With this, a POMAC can be used to compare the simulations. For more information on POD and the POMAC please refer to section 2.6. The comparison of the systems is shown in figure 4.5 and table 4.3. The energy content as displayed in the fourth column in the table is calculated as follows:

$$\text{Energy content}_i = \frac{\text{POV}_i}{\sum \text{POV}} \times 100\% \tag{4.1}$$

From the comparison, it is clear that the simulations of the Guyan and the Craig-Bampton reduced systems match closely. The first two POMs contain almost all of the energy of the system and they have a POMAC value of 1.00.

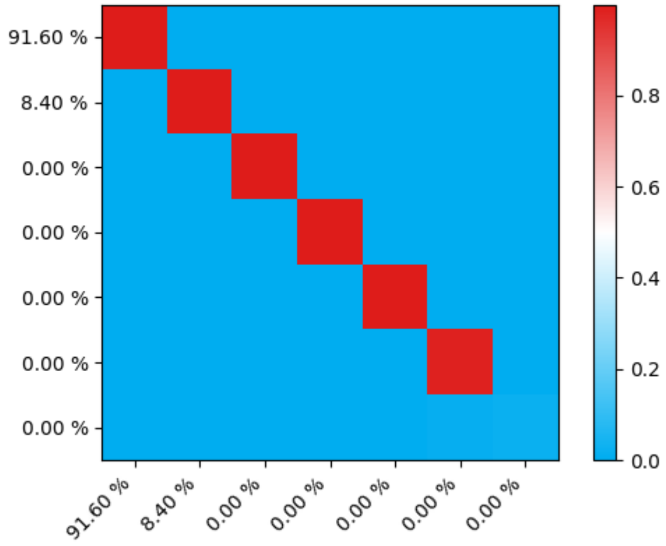

Figure 4.5: Comparison of displacement over time for the Guyan and the Craig-Bampton reduced systems with a forcing period of 3s

Table 4.3: Comparison of matched POMs of Guyan and Craig-Bapton reduced systems with a forcing period of 3s

POM pair	POMAC	POV error (%)	Energy content (%)
(1, 1)	1.00	0.02	91.60
(2, 2)	1.00	0.02	8.40
(3, 3)	1.00	0.01	0.00
(4, 4)	1.00	0.73	0.00
(5, 5)	1.00	99.26	0.00
(6, 6)	0.99	99.34	0.00
(7, 7)	0.02	99.33	0.00

5

Implementation of the system

To investigate the potential of the use of dynamic substructuring for modelling an upending hinge, the assembled model, described in chapter 4, is implemented into dynamic analysis simulations. In this chapter, this implementation is described. The upending simulations containing the substructured model are compared with conventional upending simulations to evaluate the substructured model's performance.

The chapter is organized in the following manner. In section 5.1, the general modelling approach of the upending operation simulation is discussed. This is followed in section 5.2 by the discussion of a spectral response analysis of the system. Finally, a description of an operability study using regular waves and its results is given in section 5.3.

5.1. Modelling approach

The reduced system is implemented into Marine Dynamic Analysis Software (MDAS) to describe the interaction between the MP and vessel during an upending procedure. In this software, the upending procedure is simulated in the time domain using discrete time steps. This model can vary in complexity but to assess the performance of the reduced system, the model seen in figure 5.1 is used.

The model consists of a crane vessel which is moored with 4 mooring lines and an MP that is to be upended. Attached to the crane on the ship is a hoisting wire that is in turn connected to the top of the MP. The crane is positioned such that the point at which the wire is connected to the crane is directly above the point at which the wire is connected to the MP. In other words, the resting position of the hoisting wire is vertical. The MP is, of course, also connected to the vessel through the UEH. This connection is modelled in two ways.

The first way of modelling the UEH is the one that is commonly used by TWD and does not use the reduced FEM model described in this thesis. Here, the UEH is modelled as a collection of springs and hinges. The springs and hinges each have a (rotational) stiffness that is determined from FEM models. By applying a force to the UEH and calculating the displacement as a result of this force, the stiffness of the UEH in the direction of the force can be approximated. The total behaviour of the UEH can be modelled by combining these springs and hinges as seen in 5.3a. This approach is applied to the unsimplified FEM models. From the models of the folding frames, a translational stiffness in the x, y and z directions is determined. From the models of the bucket, a translational stiffness is determined in the direction perpendicular to the MP towards the vessel. From the models of the U-frame, a rotational stiffness is determined in the plane through the length of the MP and perpendicular to the plane of the upend rotation. Also, the stiffness in the axial direction of the MP is determined from the model of the U-frame.

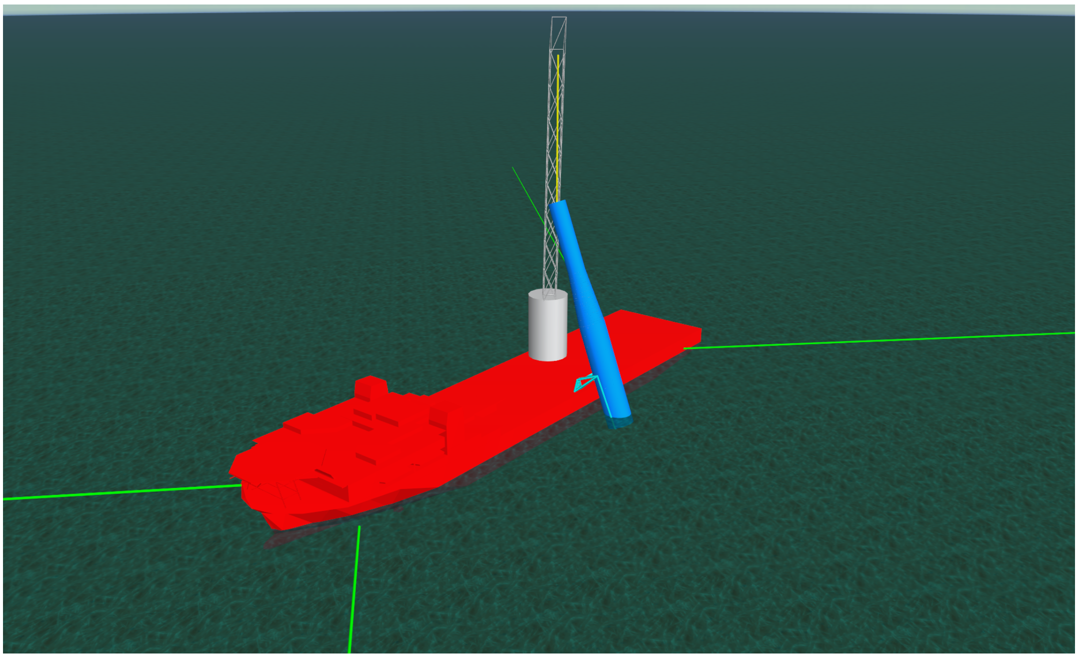

Figure 5.1: Upending model in which the reduced system is implemented

The second way of modelling the UEH, contrary to the conventional modelling approach, does use the reduced FEM model. It uses the mass and stiffness matrices acquired from the assembly described in chapter 4. The structural damping in the system is modelled as Rayleigh damping as follows:

$$\boldsymbol{C} = \alpha \boldsymbol{M} + \beta \boldsymbol{K} \tag{5.1}$$

Here $\boldsymbol{C}$ is the damping matrix and is calculated as a linear combination of $\boldsymbol{M}$ (the mass matrix) and $\boldsymbol{K}$ (the stiffness matrix). For the coefficients α and β the typical value of 0.05 is chosen. The implementation of the reduced system is not straightforward. Whereas the collection of springs can be described in the MDAS directly, the reduced FEM model must be implemented as an external function. To the MDAS, this external function is, as it were, a black box. The interaction between the MDAS and the external function is shown in figure 5.2. At every time step in the simulation, the MDAS calculates the motions of the points on the MP and vessel to which the UEH is attached. These boundary DoF motions are passed to the external function. The external function calculates two things. First, the motions of the internal DoFs are determined. This is done using an initial value problem solver that uses the Radau method; this is a Runge-Kutta method that is stable for highly stiff systems. From the motions of the internal DoFs in the previous time step, the motions of the boundary DoFs and using the mass, damping and stiffness matrices, the new motions of the internal DoFs are calculated. Then, when the motions of all DoFs are determined, the boundary forces can trivially be calculated. The boundary forces are, subsequently, returned to the MDAS and used for the calculation of the next time step. The total behaviour of the UEH can thus be schematized as shown in figure 5.3b.

As the upending procedure takes several minutes, it is modelled quasi-statically. Several simulations are run with varying static upending angles. Research by TWD concluded that for this specific upending procedure, the upending angles between 69 degrees and 87 degrees were critical. Therefore, the upending angles of 69, 78 and 87 degrees are investigated.

The goal of these simulations is to determine the loads and displacements that occur during the upending. Should they exceed certain thresholds, then the operation cannot be executed

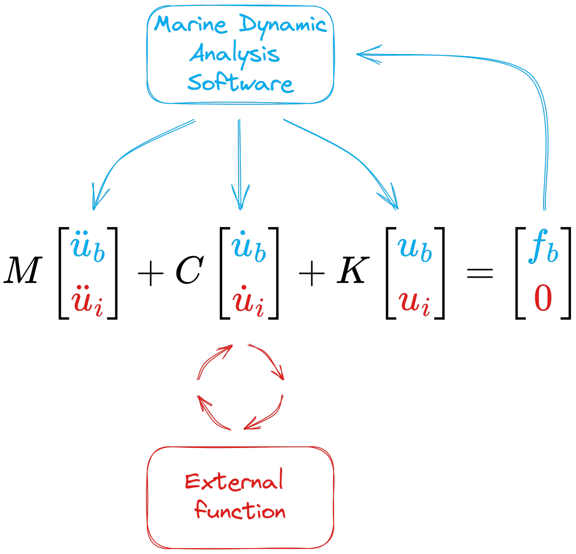

Figure 5.2: Overview of how the external function interacts with the dynamic model

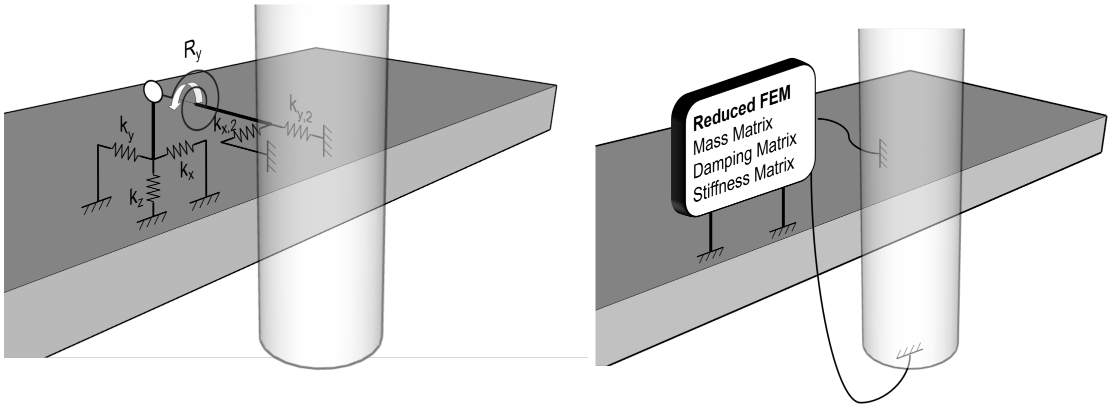

(a) Modelling the UEH as a series of springs and hinges

(b) Modelling the UEH using the reduced FEM model

Figure 5.3: Two approaches of modelling the UEH

safely. For this model, the following loads and (angular) displacements were found to be critical:

- **Crane cable tension:** If the tension in the crane cable exceeds the design load the cable might wear excessively or even fail completely.
- **Crane cable off-lead angle:** The off-lead angle is the angle of the crane cable in the plane of luffing, relative to the verticle (see figure 5.4). Cranes are designed to lift loads vertically and cannot endure large horizontal loads. Should the off-lead angle be too large it may cause a horizontal load that is too great for the crane to handle.
- **Crane cable side-lead angle:** The side-lead angle is the angle between the crane cable and the verticle in the direction perpendicular to the off-lead angle(see figure 5.4.) Similarly to the off-lead angle, a large side-lead angle may cause a critical horizontal load.
- **MP Rx rotation:** This is the rotation in the upending direction. For a safe upending procedure, the MP should not rock back and forth too much during upending

- **MP Ry rotation:** This is the rotation of the MP along the side of the ship. The plane of this rotation, rotates with the MP as it is upended. The U-frame of the UEH is relatively flexible in this direction. The resonance frequency of this motion may therefore be sufficiently low to be excited by ocean waves causing excessive loads on the UEH.

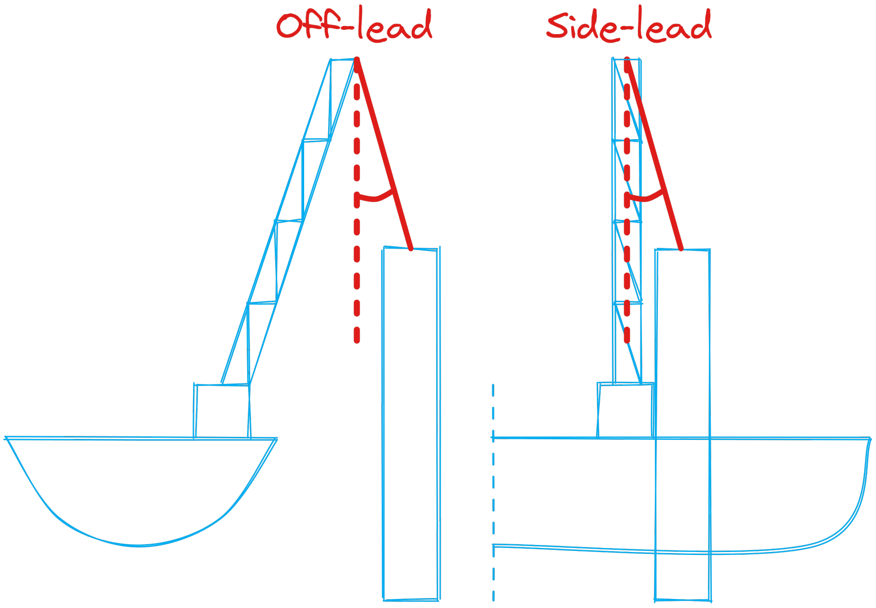

Figure 5.4: Definition of Off-lead and Side-lead of the crane cable

To compare the conventional modelling approach with the approach using the reduced FEM models, two types of simulations are run.

5.2. Spectral response analysis

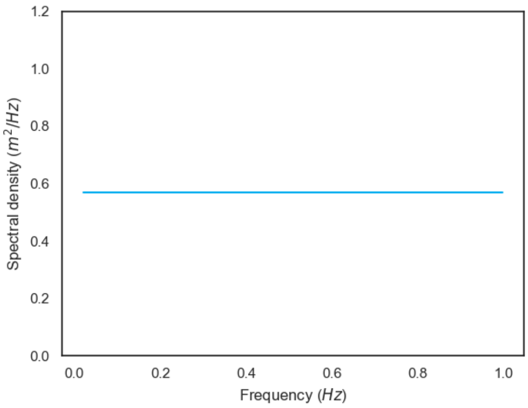

Figure 5.5: Wave spectrum that is used for spectral response analysis

The first type of simulation that is done is the spectral response analysis. The goal of this analysis is to determine the Response Amplitude Operator (RAO) for various responses of the system. This can normally be accomplished by simulating the system in the frequency domain. The system, however, contains several non-linear components such as the mooring lines. Therefore, a simple simulation in the frequency domain is not possible. The spectral response analysis solves this problem by approximating the RAOs in the time domain.

This works as follows. In the simulation, the vessel and MP are subjected to a wave spectrum with the wave energy spread evenly over a range of frequencies (Orcina, 2023). To demonstrate, the spectral density of the wave spectrum used is shown in figure 5.5. By, subsequently, applying a Fourier transform to the results of the simulation the time domain results are transformed into the frequency domain in the form of the power spectral density. Since all wave frequencies are represented equally, peaks in the power spectral density can only be caused by resonating frequencies of the system. The power spectral densities can, thus, be converted into RAOs.

The RAOs of the systems are calculated for two reasons. Firstly, the RAOs impart fundamental information on the behaviour of the system. They can therefore be used as a basis for validation of the models; does the system behave as expected? Secondly, the RAOs provide insight into the differences between the modelling approaches. This may yield valuable information into how the systems differ and why.

The following systems are simulated. For each of the upending angles of 69°, 78° and 87° three models are run:

- A model with the conventional approach for modelling an UEH
- A model that uses the Guyan-reduced model of the UEH
- A model that uses the Craig-Bampton-reduced model of the UEH

From each of these simulations the RAOs for the five responses described in section 5.1 are calculated.

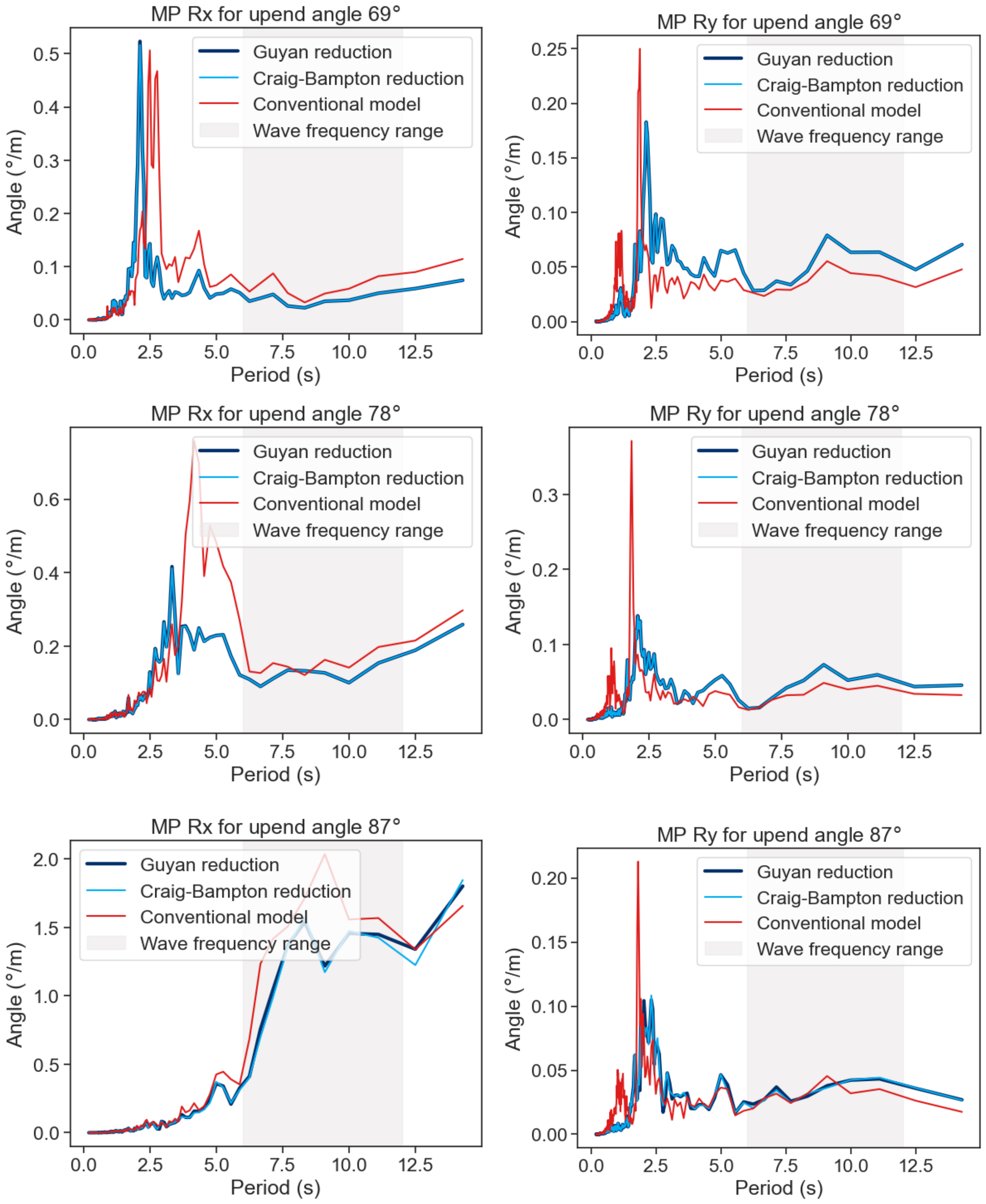

Figure 5.6: RAOs of the Rx and Ry rotations of the Monopile for the 3 upending angles

5.2.1. Analysis of the RAOs

The three different modelling approaches can now be analysed. As the Rx and Ry rotations of the MP are the main cause of the other three responses, the analysis will focus mainly on these responses. They are displayed in figure 5.6. An overview of all RAOs can be found in appendix B. It was determined that in operation, the encountered wave period range is between 6 and 12 s. This is highlighted in the figures in grey for reference. Throughout this chapter, waver periods that are lower than 6 s will be referred to as the low-period or high-frequency domain. Wave periods that are higher than 6 s will be referred to as the high-period or low-frequency domain.

Before diving into the nuances of the RAOs, there is one evident thing to note. The RAOs from the simulations using the Guyan reduction are nearly indistinguishable from the simulations using the Craig-Bampton reduction for all upending angles. This means the addition of the boundary fixed modes to the reduction basis has a marginal contribution to the overall behaviour of the model. This is to be expected as the modes were found to be of relatively high natural frequency. Hence, they are not excited by the relatively lower excitation frequencies caused by the waves. As the Guyan reduced system and the Craig-Bampton reduced systems are almost indistinguishable, from this point on, two systems will be addressed; the (dynamically) substructured system and the conventional system.

Overall dynamic behaviour

Let us start with the overall behaviour of both systems and, firstly, the response of the MP in Rx direction. It can be seen that both systems have a peak, meaning a resonance frequency, in the higher frequency domain. This peak corresponds to a natural mode of the MP hanging in the crane wire and resting on the UEH. This becomes clear by looking at figure 5.7. Here the RAO of the response of the MP in Rx direction is displayed for a system in which the vessel is fixed in place. Thus, here the response of the system cannot be caused by displacements of the vessel and only by the MP moving in the crane wire and UEH.

As the upend angle increases, the peak moves towards a lower frequency, i.e. a higher period. This is to be expected. The restoring forces of the MP are the components of gravity and the crane cable tension that are perpendicular to the MP. The lower the upend angle, the higher the angle of the MP from the vertical and thus the higher the components perpendicular to the MP are.

Furthermore, for a higher upend angle, the peak in the RAO becomes wider. This is due to the damping effect of the water on the MP. As the upend angle becomes larger, more of the MP is submerged in water. This means more of the MP is dragged through the water and more viscous drag forces act on the MP. These drag forces dampen the response of the MP and cause the peaks to widen.

Moreover, it can be seen that for high periods, the response of the Rx rotation increases. This is caused by the response of the vessel to the waves. In figure 5.8 the roll and pitch RAOs of the vessel are given. As can be seen, the RAO for the roll of the vessel is larger for longer wave periods. As the roll of the vessel has a great impact on the Rx motion of the MP, this response thus increases for higher periods. It is coherent that this increase in response is not visible in the RAOs with the vessel fixed.

The high-frequency dynamic behaviour of the rotation of the MP in the Ry direction is dominated by the stiffness of the hinge in this direction. This stiffness is significantly higher than the stiffness induced by the crane wire. The main natural frequency of the rotation of the MP in Ry direction is therefore independent of the upend angle as can be seen in figure 5.6.

For higher wave periods, the response of the Ry-rotation increases slightly. This is caused by the pitch response of the installation vessel. As can be seen in figure 5.8, the vessel pitch response increases with the wave period. The pitch response of the vessel is, however,

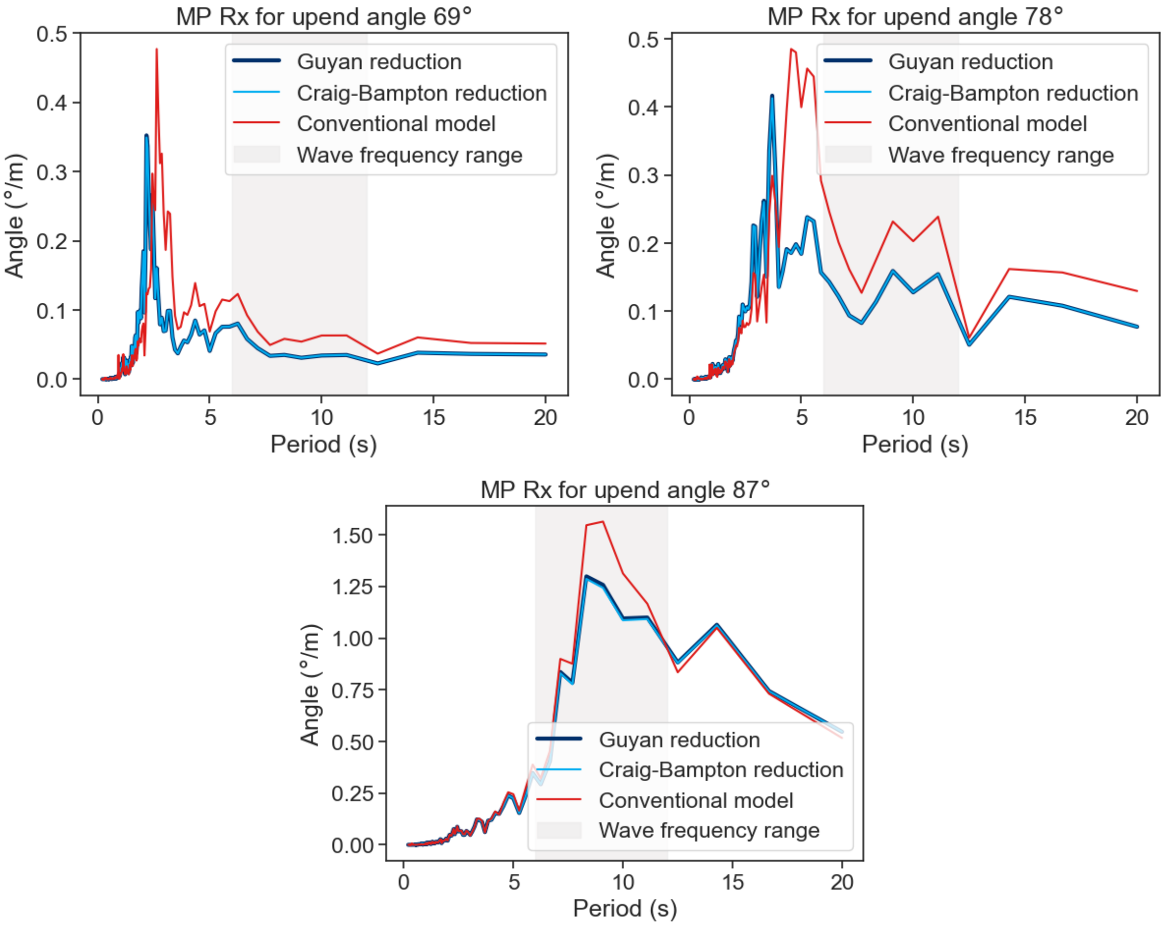

Figure 5.7: RAOs of the Rx rotation of the Monopile for the 3 upending angles with the installation vessel fixed in place

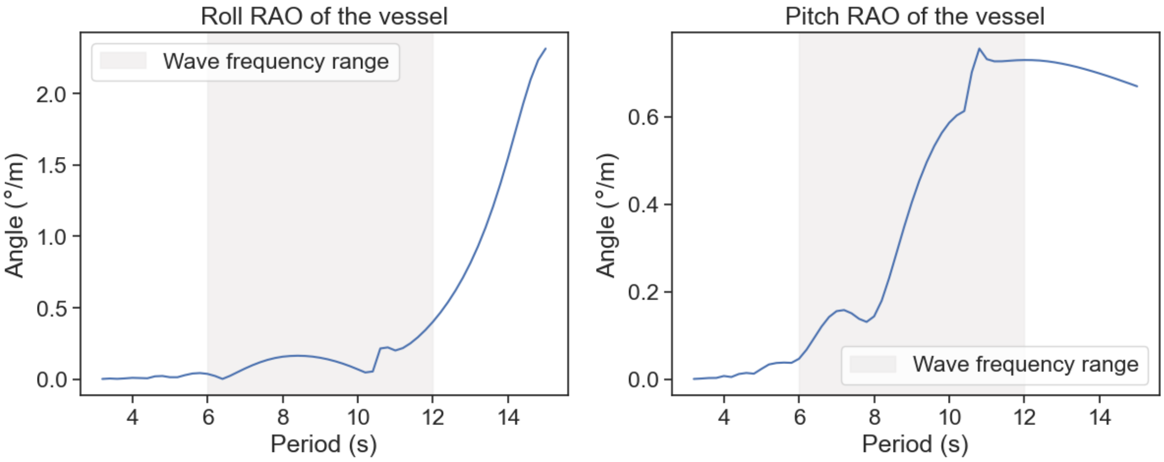

Figure 5.8: Roll and pitch RAOs of the installation vessel

significantly lower than the roll response of the vessel. The effect of the vessel on the low frequency RAOs of the MP is therefore greater for the Rx-rotation than for the Ry-rotation.

The fact that the general shapes of the RAOs of both systems are similar contributes to the validation of the substructured model. Furthermore, the shape of the RAOs can be explained by several properties of the system as described above, adding further to the validation of the model.

Differences between the modelling approaches

Even though the responses of the systems are quite similar, there are several notable differences. It is important to identify these differences and try to explain them. To aid with explaining the differences, first, a simple system is described. The aim of this system is to explain the effect of neglecting the mass of the upend hinge in the conventional approach. Because the simple model is less complex than the model of the UEH, it is easier to isolate and explain this effect. The system is shown in figure 5.9a. The meaning of figure 5.9b will be explained shortly.

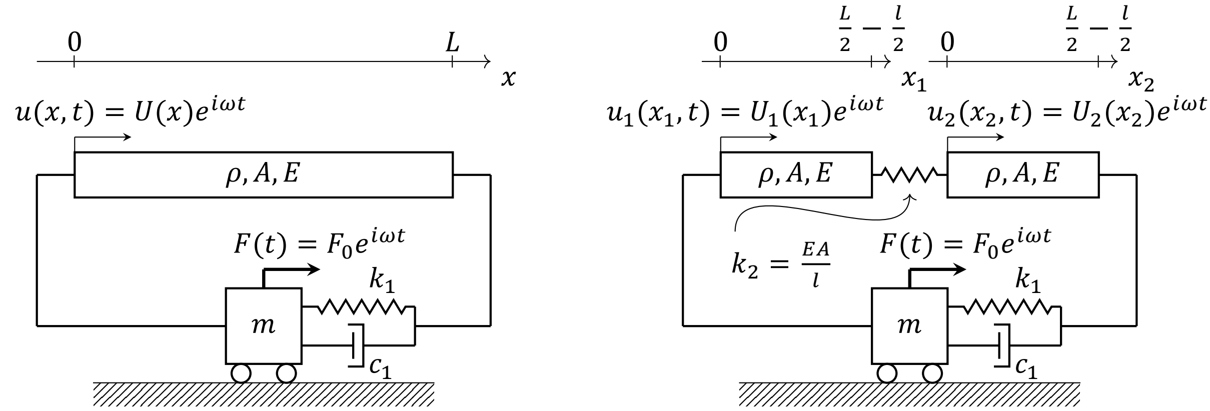

(a) Original model

(b) Model in which part of the beam has been replaced by a spring

Figure 5.9: Simple model of a connected mass and beam, modelled in two ways.

The system consists of a point mass with mass m and a flexible beam. The beam can deform in x direction and has a length L, a density ρ, a cross-sectional area A and a Young's modulus E. The beam is connected in two ways to the point mass. On the left-hand side, it is connected rigidly. This means the left-hand side of the beam has the same displacement as the point mass. On the right-hand side, it is connected via a spring-damper system with stiffness k_1 and damping coefficient c_1. The point mass is excited by a harmonic force $F(t)$ with amplitude F_0 and frequency ω. As the system is linear, the beam will displace ($u(x,t)$) at the same frequency ω but with a different complex amplitude $U(x)$.

The model displayed in figure 5.9b is the same model as just described but here a part of the flexible beam is snipped out and replaced with a simple spring with the same stiffness as the part of the beam that it replaces. The part that is cut out has a length l and is located in the middle of the beam. This results in a system with two degrees of freedom instead of one.

The two models can be used to represent the substructured approach of modelling the hinge and the conventional approach. In the substructured approach, the mass of UEH is taken into account, similar to the model shown in figure 5.9a. In the conventional approach of modelling the UEH, the mass is neglected and it can thus be represented by the model shown in figure 5.9b.

Both models of the simple system can be solved analytically. The derivations of the reponses are shown in appendix C. The chosen values of the various parameters are shown in table 5.1. The values of the parameters are for the most part arbitrary. A notable exception, however, is the relatively high mass of the point mass compared to the mass of the beam. This is chosen as such to analogize the vessel that is significantly heavier than the UEH and MP.

Table 5.1: Values of the various parameters of the simple system

Parameter	Value
L	3 m
l	0.75 m
ρ	8000 kg/m^3
A	0.01 m^2
E	4E3 Pa
$k1$	200 N/m
$C1$	10 Ns/m
m	1E6 kg

In figure 5.10 a comparison of the response of the continuous and the snipped models is given. On the y-axis is given the absolute value of the amplitude of the displacement of the right-hand side of the beam, divided by the amplitude of the forcing. On the x-axis is the period of excitation. It can be seen that the response of both models is indistinguishable for lower frequencies of excitation. Even though part of the mass of the beam is neglected in the model with the snipped beam, this does not have an effect on the low-frequency response. It does, however, have an effect on the high-frequency response. As can be seen in the figure, the frequency at which the response peaks is different for both models. The model with the snipped beam has a mode with an eigenperiod that is lower than the eigenperiod of the mode of the non-snipped model. Due to the reduction in mass in the snipped beam, its dynamic behaviour is stiffer than the continuous beam.

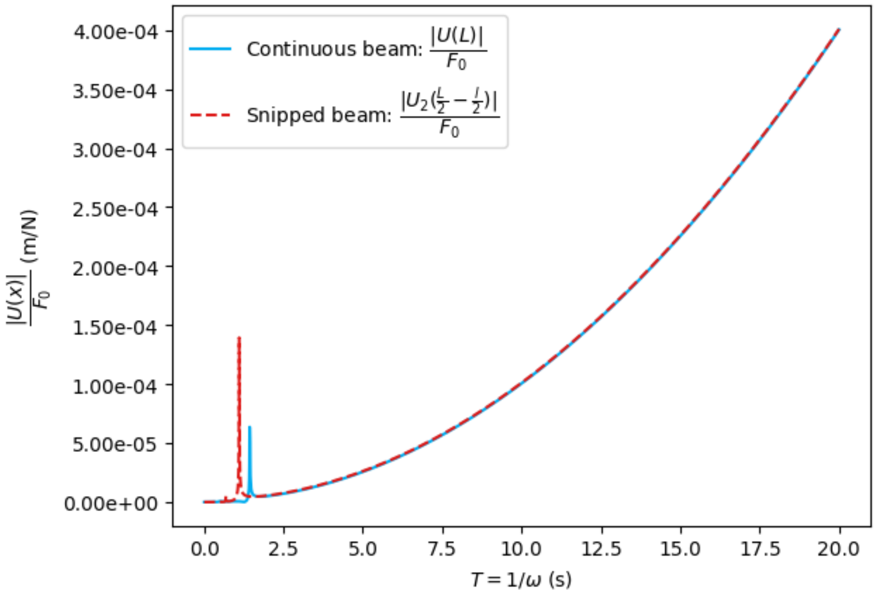

Figure 5.10: Relative amplitude of the displacement of the right-hand side of the beam for both the continuous and the snipped models

This general behaviour can also be seen in the RAOs of the Ry rotation of the MP. The biggest differences can be seen in the high-frequency domain. Similarly to the snipped-beam variant of the simple model, the response of the conventional model peaks at a lower period than the response of the substructured system. This can be explained by the fact that the substructured system takes the mass of the UEH into account.

The low-frequency response of the Ry rotation of the MP is higher for the substructured system than for the conventional system. A possible explanation for this can be found in the manner in which the stiffnesses of the springs for the conventional system are found. As discussed previously, the stiffnesses are determined by applying a force to the FEM model of the UEH in a certain direction and calculating the caused displacement in that same direction. This approach, however, fails to take into account the coupling stiffness. Due to a force in one direction, the UEH may deform, partly, in another direction. By failing to take this into account in the conventional model, the system becomes stiffer than it should be. As the low-frequency response of the Ry rotation of the MP is dominated by the pitch motion of the vessel, it is highly dependent on the stiffness of the hinge. It can be said that in low-frequency conditions, the MP is dragged back and forth by the vessel; it follows the motion of the vessel. Thus, if the UEH is stiffer, the response will be lower as the MP will follow the vessel more closely.

For the rotation of the MP in Rx direction, the biggest differences between the substructured and the conventional systems can again be seen in the high-frequency domain. As this rotation is not supposed to be inhibited by the hinge, both models of the hinge should have no stiffness in this direction. Hence, a difference between the responses is unexpected. Nevertheless, in the RAOs of the MP rotation in Rx direction, there is a significant difference between the two systems. The response of the conventional model is higher and the natural period of the most significant peak is higher than in the substructured system. A potential explanation, however, lies in the linearity of the FEM models on which the substructured models are based. The consequence of this is that rotations are approximated using the small-angle approximation. Thus, the displacement of the bottom of the U-frame due to the free rotation of the UEH is approximated as a straight line. The rotation of the MP, however, is not linearised. Even though the angles are small and the discrepancies should thus be small as well, due to the fact that the overall system is very stiff, a small difference in displacement can cause a significant force. As, in the conventional system, no small angle approximation is applied, this effect is non-existent for this system. This additional stiffness in the hinge would explain both the lower natural frequency and the lower response of the substructured system compared to the conventional system.

To explore this effect further, another analogical model is described. The model, shown in figure 5.11, consists of a rigid pendulum with a mass m and a length l. At the pivot point, the pendulum is subject to a rotational stiffness k_r, a rotational stiffness c_r and a sinusoidal moment M with angular frequency ω. A platform is also rigidly attached to this pivot point. It can freely rotate around the pivot. The platform and the mass are connected with a stiff linear spring with stiffness k. Gravity is neglected in this model.

The system is modelled with a non-linearised rotation of the platform (shown in figure 5.11a) and a linearised rotation of the platform(shown in figure 5.11b). In the model with the non-linearised rotation, the spring at the bottom remains unstretched. In the model with the linearised rotation, however, the spring is stretched. The platform with the spring represents the UEH. The pendulum with the non-linearised rotation of the platform represents the conventional model of the UEH and the pendulum with the linearised rotation represents the substructured model of the UEH.

For both models, the steady-state amplitude of θ (relative to M_0) is determined as a function of the period of moment M. The chosen values for the variables are displayed in table 5.2. The resulting RAOs of θ are displayed in figure 5.12.

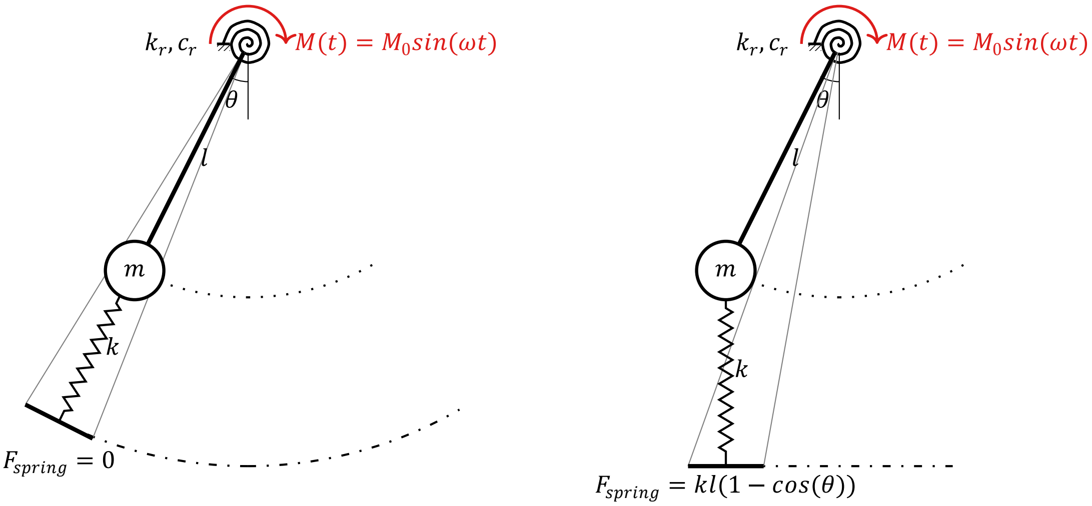

(a) Pendulum with non-linearised rotation of the stiffness (b) Pendulum with linearised rotation of the stiffness

Figure 5.11: Model of a pendulum with a linearised rotation and a non-linearised rotation of the stiffness

Table 5.2: Values of the various parameters of the model of the pendulum

Parameter	Value
m	100 kg
l	3 m
k	1000 kN/m
k_r	200 Nm/rad
c_r	100 Nms/rad
M_0	0.25 Nm

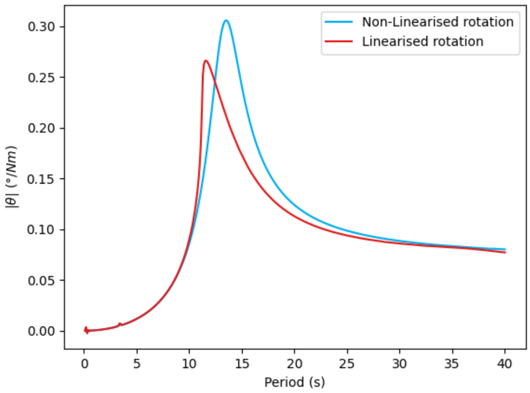

Figure 5.12: Comparison of the response of a non-linearised and a linearised model of a pendulum

As can be seen in figure 5.12, the linearisation of the rotation, introduces a stiffness in the system. This causes the peak of the response spectrum to shift to lower periods. Furthermore, it can be seen that the high-period response is lower for the system with the linearised rotation. This is in line with the difference in response of the conventional and the substructed system as described earlier. It is therefore conceivable that the difference can, in part, be explained by the effect of the linearisation of angles.

5.2.2. Intermediate conclusions of the spectral response analysis

Two main intermediate conclusions can be drawn from the performed spectral response analysis. The first is concerning the validity of the substructured system. In a general sense, the dynamic behaviour of the system is as expected. It can be explained by the properties of the entire system. Furthermore, the response of the substructured system is not exceedingly different from the response of the conventional system. This reinforces the validity of substructured system. The second conclusion is that even though the response of both systems is quite similar, there are several noticeable differences. For each of these differences, an explanation is put forward. These explanations mostly imply that the substructured system describes a response that is closer to reality.

5.3. Regular wave simulations

The second type of analysis that is done is one where the vessel and MP are subjected to a variety of regular waves. For each simulation, the waves have a different direction and period. Such a series of simulations is often used in order to determine the operability of a certain operation. For every simulation, the maximum values of critical loads and displacements are determined. Only the cases where these critical loads and displacements do not exceed their set limits are deemed operable.

For the purpose of this thesis, the question under which the upending operation can safely be performed is not important. The interest lies in the differences between the approaches of modelling the UEH. The limits of the critical loads and displacements are therefore not discussed.

The batch of simulations that is run consists of the combinations of different values of the following parameters:

- **Wave direction:** In the simulations, the vessel and MP are subjected to waves from a constant direction. The three chosen wave directions are head waves, bow quartering waves and beam waves. This corresponds to a wave heading of 180°, 225°, and 270°, respectively, as can be seen in figure 5.13. These directions are chosen to capture the behaviour of the system in pitch-dominated, roll-dominated and combined conditions.

- **Wave period:** The wave periods are chosen based on the expected conditions at the location of operation. The system is subjected to regular waves with a period of 6, 8, 10 and 12 seconds.

- **Upend angle:** Similarly to for the spectral response analysis, the upending angles of 69°, 78°and 87° are simulated.

- **UEH modelling method:** The UEH is modelled either through the implementation of the Guyan reduction or through the conventional approach as described in section 5.1. In all simulations, the wave height is 2m.

Thus, in total 72 models are run. To avoid capturing transients and effects caused by slightly imperfect starting conditions, the waves are gradually introduced into the system.

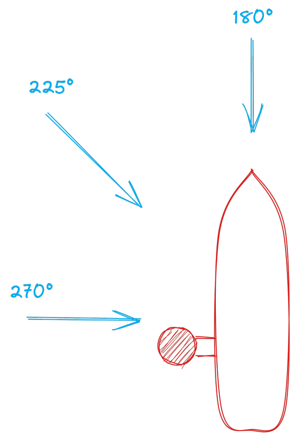

Figure 5.13: Definition of wave directions to which the system is subtjected

When the system has entered its steady state, the five critical responses are recorded over a time of one minute and the maximum value is determined. It can be seen in the example given in figure 5.14 that a time window of one minute is long enough to get a representative maximum value of the steady-state response.

5.3.1. Analysis of the dynamic response

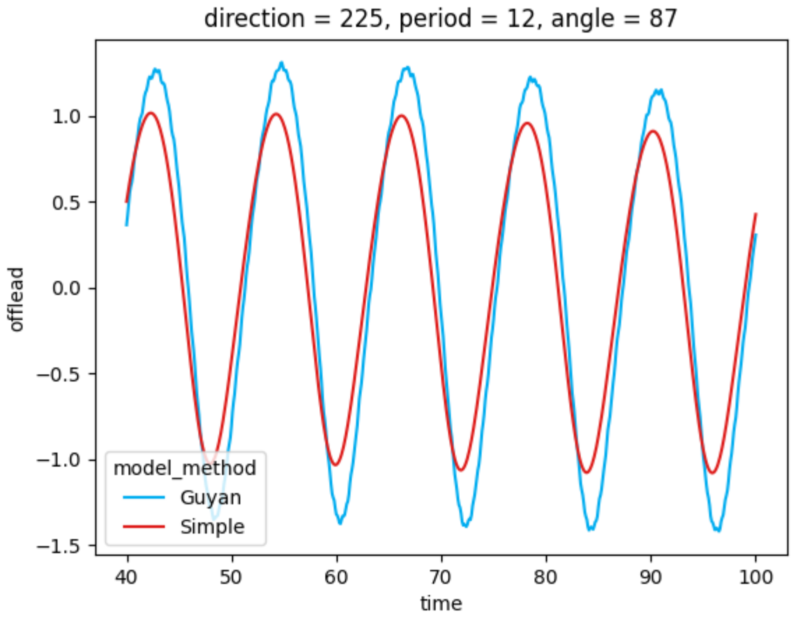

Figure 5.14: Example of the cable tension as a function of time in steady state. The results from the model using the Guyan reduction and the conventional (Simple) method are shown. It is clear that even for the longest wave period, a time window of one minute is adequate to determine a representative result.

The maximum values of the responses for all wave conditions using either the Guyan reduced system or the conventional approach are shown in table 5.3. The values correspond to the upend angle yielding the highest value. An overview of which upend angle yields the highest value for each response and wave condition is given in table 5.4.

The first thing to note is that the results from the regular wave simulations match well

Table 5.3: Maximum values of key responses for a range of wave environmental conditions. For each loading condition, if the Guyan method yields a higher value than the conventional method, it is coloured in blue. If the conventional method yields a higher response value, it is shown in red.

Wave direction	Wave period	Method	Tension (kN)	Offlead (°)	Sidelead (°)	MP Rx (°)	MP Ry (°)
180°	**6 s**	**Guyan**	1.17E+04	0.055	0.058	0.016	0.027
		Conventional	1.25E+04	0.029	0.027	0.023	0.018
	8 s	**Guyan**	1.17E+04	0.079	0.085	0.032	0.036
		Conventional	1.26E+04	0.042	0.068	0.034	0.024
	10 s	**Guyan**	1.22E+04	0.242	0.165	0.178	0.019
		Conventional	1.29E+04	0.177	0.127	0.143	0.012
	12 s	**Guyan**	1.20E+04	0.147	0.148	0.115	0.031
		Conventional	1.27E+04	0.095	0.107	0.087	0.019
225°	**6 s**	**Guyan**	1.24E+04	0.317	0.190	0.223	0.023
		Conventional	1.32E+04	0.337	0.187	0.253	0.015
	8 s	**Guyan**	1.30E+04	0.544	0.280	0.400	0.007
		Conventional	1.38E+04	0.561	0.295	0.433	0.004
	10 s	**Guyan**	1.34E+04	0.647	0.416	0.491	0.043
		Conventional	1.37E+04	0.546	0.348	0.430	0.025
	12 s	**Guyan**	1.56E+04	1.420	0.782	1.024	0.050
		Conventional	1.48E+04	1.080	0.597	0.809	0.030
270°	**6 s**	**Guyan**	1.34E+04	0.715	0.357	0.497	0.008
		Conventional	1.39E+04	0.739	0.365	0.536	0.005
	8 s	**Guyan**	1.59E+04	1.522	0.741	1.053	0.009
		Conventional	1.69E+04	1.876	0.919	1.376	0.006
	10 s	**Guyan**	1.91E+04	2.393	1.185	1.594	0.003
		Conventional	1.81E+04	2.383	1.182	1.749	0.001
	12 s	**Guyan**	2.10E+04	2.668	1.325	1.754	0.002
		Conventional	1.90E+04	2.650	1.319	1.943	0.002

Table 5.4: Upending angles where the maximum values of the key responses occur.

Wave direction	**Wave period**	**Method**	**Tension**	**Offlead**	**Sidelead**	**MP Rx**	**MP Ry**
180°	**6 s**	**Guyan**	87°	69°	78°	78°	78°
		Conventional	87°	78°	78°	78°	87°
	8 s	**Guyan**	87°	69°	78°	87°	78°
		Conventional	87°	69°	87°	87°	87°
	10 s	**Guyan**	87°	87°	87°	87°	78°
		Conventional	87°	87°	87°	87°	87°
	12 s	**Guyan**	87°	87°	87°	87°	78°
		Conventional	87°	87°	87°	87°	87°
225°	**6 s**	**Guyan**	87°	87°	87°	87°	78°
		Conventional	87°	87°	87°	87°	87°
	8 s	**Guyan**	87°	87°	87°	87°	69°
		Conventional	87°	87°	87°	87°	69°
	10 s	**Guyan**	87°	87°	87°	87°	78°
		Conventional	87°	87°	87°	87°	87°
	12 s	**Guyan**	87°	87°	87°	87°	78°
		Conventional	87°	87°	87°	87°	87°
270°	**6 s**	**Guyan**	87°	87°	87°	87°	69°
		Conventional	87°	87°	87°	87°	78°
	8 s	**Guyan**	87°	87°	87°	87°	69°
		Conventional	87°	87°	87°	87°	69°
	10 s	**Guyan**	87°	87°	87°	87°	87°
		Conventional	87°	87°	87°	87°	87°
	12 s	**Guyan**	87°	87°	87°	87°	87°
		Conventional	87°	87°	87°	87°	87°

with the results from the spectral response analysis. As the wave height of the waves is 2 m, the wave amplitude is 1m. This means that the expected response of the regular wave simulations is equal to the RAO corresponding to that response and period. There are some small differences between the RAOs and the responses of the regular wave simulations but those are likely due to the numerical nature of the spectral response analysis.

Furthermore, it can be seen that the effect of the wave direction on the responses is to be expected. It was already previously noted that the rotation of the MP in the Rx direction is dominated by the roll motions of the vessel. This can be seen in the fact that the responses are largest for beam waves (a wave angle of 270°. As the rotation of the MP in the Ry direction is dominated by pitch motions, this response is quite low for beam waves.

More interesting, however, are the differences in the responses of the two different modelling approaches of the UEH. In table 5.3 the responses that are higher for the Guyan-reduced model are coloured in blue. The responses that are higher for the conventional method are coloured in red. Most of the highest responses for both methods can be found in beam waves for the wave periods of 12 seconds and (as can be seen in table 5.4) for an upend angle of 87°. As the main interest of an operability study is in the highest responses, this is where the difference in response of both models is most relevant. For these sea conditions, there is a small difference between the modelling approaches. This is also in line with the RAO plots for this sea state. It can be seen that for a wave period of 12 seconds and an upend angle of 87° the RAO of the substructured and the conventional methods are almost the same.

The only response that is not highest for beam waves and a period of 12 seconds is the rotation of the MP in the Ry direction. This is highest for quartering waves (a wave angle of 225°) and a wave period of 12 seconds. Here the difference in response is significant. The substructured system produces a higher response. This is again in line with the RAOs. As discussed previously, this is most likely due to the fact that the substructured system takes coupling stiffness into account whereas the conventional approach does not. This makes the conventional system stiffer and thus it produces lower responses in the relatively low-frequency domain.

One important property of the substructured model that cannot be seen in the results that are shown so far is the simulation time. As described earlier, the substructured model of the UEH is implemented into the MDAS as an external function. The MDAS has no knowledge of how the boundary forces are calculated by the external function. More specifically, the MDAS has no knowledge of the first-order partial derivatives of the external function. For motions calculated by the MDAS itself, it uses the first-order partial derivatives between each time step to guide the solver to the system's dynamic equilibrium. For the external function, the MDAS tries to approximate its partial derivatives to arrive at a dynamic equilibrium. This leads to what could be described to some extent as a blunderbuss approach. The MDAS iterates a great number of times until it has found the system's dynamic equilibrium. This approach only works if the time step is sufficiently small. The combination of the necessity of a smaller time step, together with the large number of iterations causes the substructured system to be roughly 10 slower than the conventional model. Currently, an operability study already requires a substantial amount of processing power. Increasing this tenfold, therefore, poses a significant obstacle to the implementation of the substructured model of the UEH.

5.3.2. Intermediate conclusions of the regular wave simulations

The response of the regular wave simulations is in line with the response of the spectral response analysis. For most responses, the difference between the two modelling approaches is minimal. The only exception is the rotation of the MP in Ry direction. This response is significantly lower for the conventional approach than for the substructured approach. This is most likely due to the fact that coupling stiffness is not taken into account in the conventional approach. Furthermore, the computation time of the models using the substructured model of the UEH is roughly 10 times higher than the computation time using the conventional approach.

6

Conclusions and Recommendations

In this chapter, a reflection is presented on the achieved results. They will be used to try to answer the research questions which were posed in section 1.3 and which are repeated here:

1. **How can Dynamic Substructuring be used to model an Upend Hinge in hydrodynamic simulations of a monopile upending operation?**
2. **How does the approach using Dynamic Substructuring compare to the conventional approach in terms of computation time and accuracy?**

Hereafter, based on the conclusions, several recommendations and suggestions for future research will be given.

6.1. Conclusions

To address the first research question, the process of modelling the UEH is split into two distinct stages. The first stage is the simplification, reduction and assembly of the FEM models of the UEH. The second stage is the implementation of the dynamically substructured model of the UEH into hydrodynamic simulations.

From the first stage, it can be concluded that it is possible to produce a sufficiently reduced model, from FEM models of the UEH, that can be implemented into a hydrodynamic simulation. Both a Guyan reduction and a Craig-Bampton reduction were applied to the models of the UEH. It was found that the use of a Craig-Bampton reduction (which results in more DoFs than the Guyan reduction) added negligibly to the response of the system to typical wave frequencies when compared to the use of the Guyan reduction. It can therefore be concluded that for the UEH and wave conditions specified in this thesis, the use of a Craig-Bampton reduction is superfluous and that a Guyan reduced system describes the dynamic behaviour equally.

From the second stage, it can be concluded that a dynamically substructured model of an UEH can be successfully implemented into a hydrodynamic simulation. This can be done by implementing it into an existing hydrodynamic model as an external function. This external function takes as input, from the Marine Dynamic Analysis Software (MDAS), the motions of the boundary DoFs where the vessel and MP interface with the UEH. In this external function, at each time step, the new internal DoF motions are calculated from the internal DoF motions of the previous time step and the boundary motions provided to the function by the MDAS. Subsequently, the boundary forces that the UEH exerts on the MP and vessel are calculated. This approach to implementing the substructured model gives a hydrodynamic simulation that behaves as expected.

This, then, answers the first research question. This thesis describes a successful approach in which models of an upend hinge can be reduced using Dynamic Substructuring and subsequently implemented into hydrodynamic simulations of an upend operation.

To answer the second research question, two types of hydrodynamic simulations have been performed using both the conventional approach of modelling a UEH and the Dynamic Substructuring approach described in this thesis. The first type is a spectral response analysis and the second type is an operability study using Airy waves. There are several things to note regarding the differences between the results using the conventional and the Dynamic Substructuring approach.

The first conclusion that can be drawn is that the computation time of the simulations using the substructured model of the UEH is significantly larger than the computation time of the conventional simulations. To run a simulation using the substructured model takes roughly 10 times longer than the same simulation using the conventional approach. This is a severe disadvantage of the Dynamic Substructuring approach, as operability studies using the conventional method already take a significant time to complete.

The second conclusion that can be drawn is that the high-frequency response of the conventional models differs significantly from that of the substructured models. These differences can be explained by the fact that the Dynamic Substructuring approach models the dynamic properties of the system more completely. However, the high-frequency response of the system does not play a big role in the response of the system to the relatively low-frequent ocean waves. The difference between the high-frequency responses of the two differently modelled systems is, therefore, not of great importance for upending operability studies.

The third conclusion that can be drawn is more important. The low-frequency response (an excitation period between 6 and 12 seconds) of the substructured models differs little from that of the conventional models. As the conditions in which the UEH operates are predominantly low-frequent ocean wave conditions, this is the most relevant frequency domain.

So, to answer the second research question. The approach using Dynamic Substructuring has a significantly higher computation time than the conventional approach. Even though the accuracy of the high-frequency response of the Dynamic Substructuring approach is higher than the high-frequency response of the conventional approach, there is little difference between the responses in the low-frequency domain. As this is the main frequency range in which the UEH operates, it is most relevant for operability studies.

6.2. Recommendations & Future Research

Based on the presented conclusions, it is not recommended to apply Dynamic Substructuring to model an upend hinge in the manner described in this thesis. The accuracy that is gained by applying this method for operability studies is insignificant. Especially considering the fact that this approach increases the computation time tenfold, not even factoring in the time needed to construct the dynamically substructured model.

However, it may be valuable to apply Dynamic Substructuring in situations where the high-frequency behaviour is relevant. This can be in simulations of, for example, the piling of monopiles or other heavy impact-related operations. Here a more accurate description of the high-frequency behaviour may prove worthwhile.

Furthermore, if it were possible to bring down the computation time of the simulations in which Dynamic Substructuring is applied, they would be more viable. There are several ways in which this might be possible. Firstly, it may be possible to improve the implementation of the substructured model into the MDAS. By determining a method to communicate the partial derivates of the external function to the MDAS, the dynamic equilibrium may be found more quickly, increasing the computational speed.

Secondly, it was shown in section 5.2 that the mass of the UEH has little effect on the low-frequency response of the system. It may therefore be sufficient to determine the boundary forces exerted by the UEH solely by its displacement and stiffness. This should significantly reduce computation time as the system that is solved by the external function becomes less complex.

An additional potential field of future research is the application of Dynamic Substructuring, not to determine operability, but to determine fatigue. As it is trivial to extract forces from the substructured models, this information may be used to determine load cycles of for example sea fastening. Here Dynamic substructuring could be a powerful tool to more accurately determine the fatigue life of offshore equipment.

Bibliography

Bilgili, M., Alphan, H., & Ilhan, A. (2022). Potential visibility, growth, and technological innovation in offshore wind turbines installed in europe. *Environmental Science and Pollution Research*. https://doi.org/10.1007/s11356-022-24142-x

Craig, R. R., & Bampton, M. C. C. (1968). Coupling of substructures for dynamic analyses. *AIAA Journal*, *6*(7), 1313–1319. https://doi.org/10.2514/3.4741

Falnes, J. (2002). Ocean waves and oscillating systems. *Ocean Waves and Oscillating Systems, by Johannes Falnes, pp. 286. ISBN 0521782112. Cambridge, UK: Cambridge University Press, April 2002.*, *-1*. https://doi.org/10.1017/CBO9780511754630

Guyan, R. J. (1965). Reduction of stiffness and mass matrices. *AIAA Journal*, *3*(2), 380–380. https://doi.org/10.2514/3.2874

Helfrich, R., & Marchesini, J. (n.d.). Dynamic substructuring with mixed boundary conditions to cope with complex structural assemblies. *727*, 56. https://ui.adsabs.harvard.edu/abs/2014ESASP.727E..56H

IRENA. (2022). *Renewable energy statistics 2022* (Report No. 978-92-9260-446-2).

Klerk, D., Rixen, D., & Voormeeren, S. (2008). General framework for dynamic substructuring: History, review, and classification of techniques. *Aiaa Journal - AIAA J*, *46*, 1169–1181. https://doi.org/10.2514/1.33274

Li, Y., Hu, S.-L., Wang, J., & Huang, Z.-H. (2020). An introduction to the computational complexity of matrix multiplication. *Journal of the Operations Research Society of China*, *8*(1), 29–43. https://doi.org/10.1007/s40305-019-00280-x

Liang, Y. C., Lee, H. P., Lim, S. P., Lin, W. Z., Lee, K. H., & Wu, C. G. (2002). Proper orthogonal decomposition and its applications—part i: Theory. *Journal of Sound and Vibration*, *252*(3), 527–544. https://doi.org/https://doi.org/10.1006/jsvi.2001.4041

Lyu, Y. (2022). Finite element method : Element solutions. https://doi.org/10.1007/978-981-19-3363-9

Mechanical apdl 2023 r1 element reference. (2023). https://ansyshelp.ansys.com/account/secured?returnurl=/Views/Secured/corp/v231/en/ans_elem/Hlp_E_ElemTOC.html

Offshore wind in europe - key trends and statistics 2020 (Report). (2021).

Orcina. (2023). Spectral response analysis. https://www.orcina.com/webhelp/OrcaFlex/Content/html/Spectralresponseanalysis.htm

Pastor, M., Binda, M., & Harčarik, T. (2012). Modal assurance criterion. *Procedia Engineering*, *48*, 543–548. https://doi.org/https://doi.org/10.1016/j.proeng.2012.09.551

Rao, S. S. (2004). *Mechanical vibrations si* (4th ed.). Addison Wesley.

Rixen, D. J. (2007). *Lecture notes, numerical methods in engineering dynamics*.

Sánchez, S., López-Gutiérrez, J.-S., Negro, V., & Esteban, M. D. (2019). Foundations in offshore wind farms: Evolution, characteristics and range of use. analysis of main dimensional parameters in monopile foundations. *Journal of Marine Science and Engineering*, *7*(12), 441. https://doi.org/10.3390/jmse7120441

TWD Japan. (2023). Upending hinge. https://www.twdjapan.co.jp/en/contents/build-up/

Voormeeren, S. (2012). *Dynamic substructuring methodologies for integrated dynamic analysis of wind turbines* (Thesis). https://doi.org/https://doi.org/10.4233/uuid:f45f0548-d5ec-46aa-be7e-7f1c2b57590d

A

MAC plots Simplification

The following figures show the MAC plots for the original and simplified models of the components of the UEH.

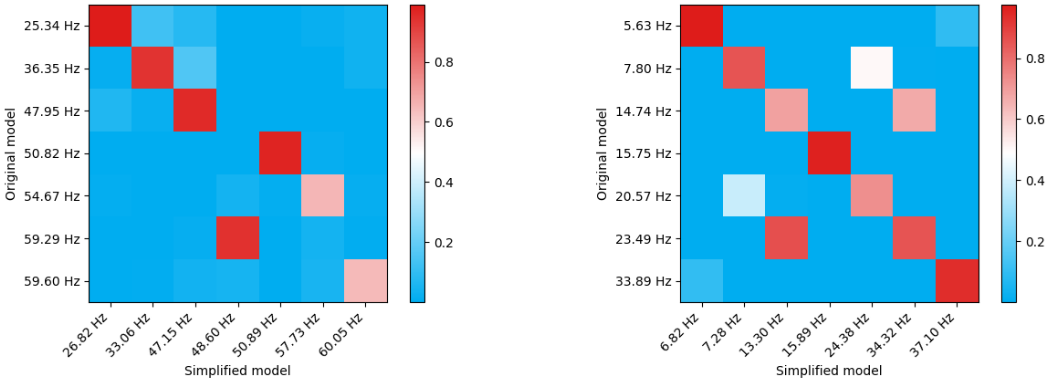

(a) MAC plot for original and simplified Folding frame model (b) MAC plot for original and simplified Bucket model

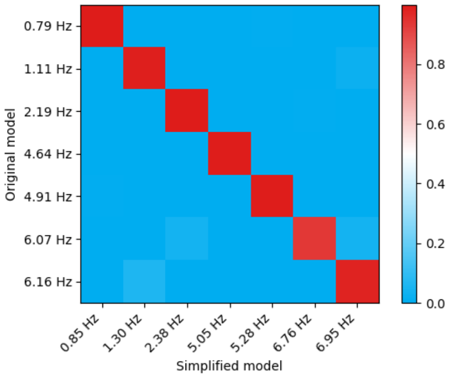

(c) MAC plot for original and simplified U-frame model

B

RAOs from spectral response analysis

The following figures show the RAOs from the spectral response analysis of the different models. The wave frequency range that was found to be prevalent in the location of operation is shaded in grey.

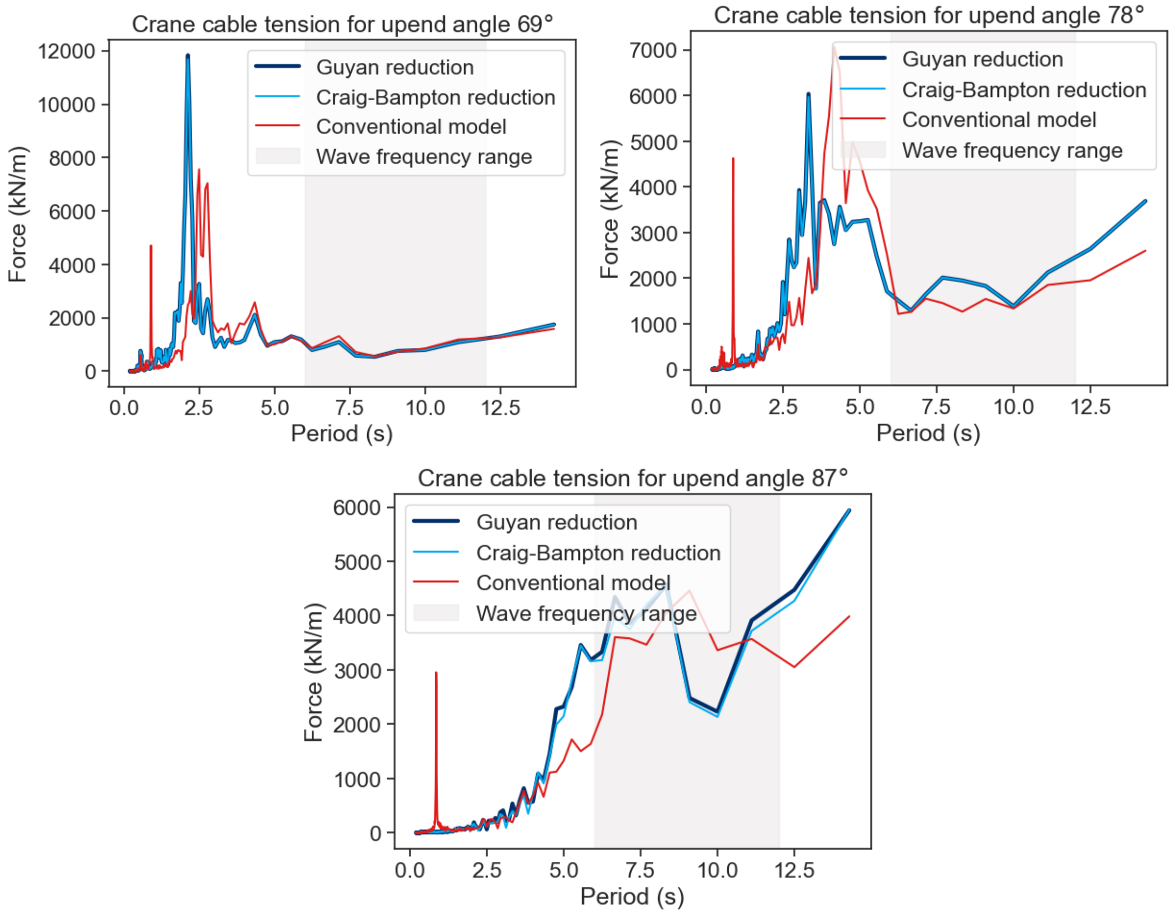

Figure B.1: RAOs of the crane cable tension for the 3 upending angles

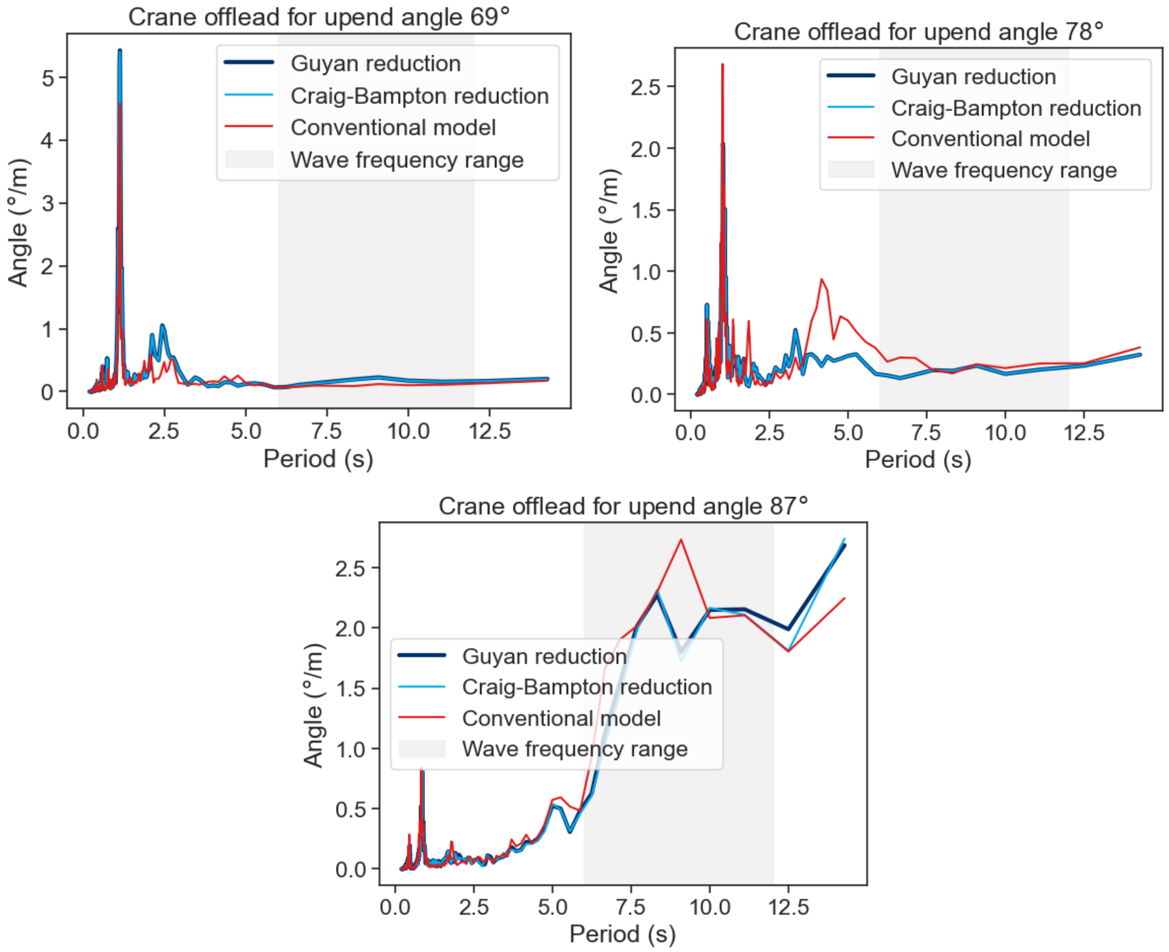

Figure B.2: RAOs of the crane offlead for the 3 upending angles

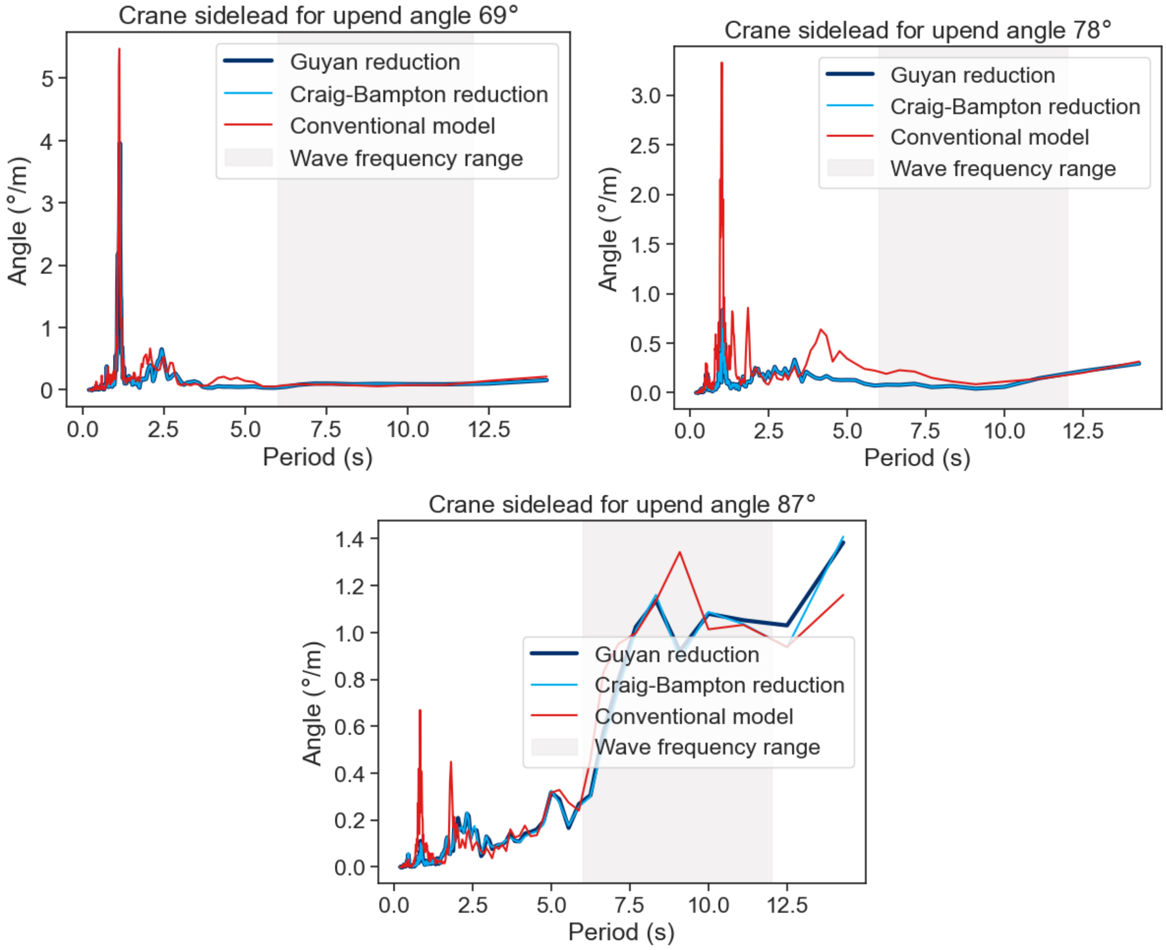

Figure B.3: RAOs of the crane sidelead for the 3 upending angles

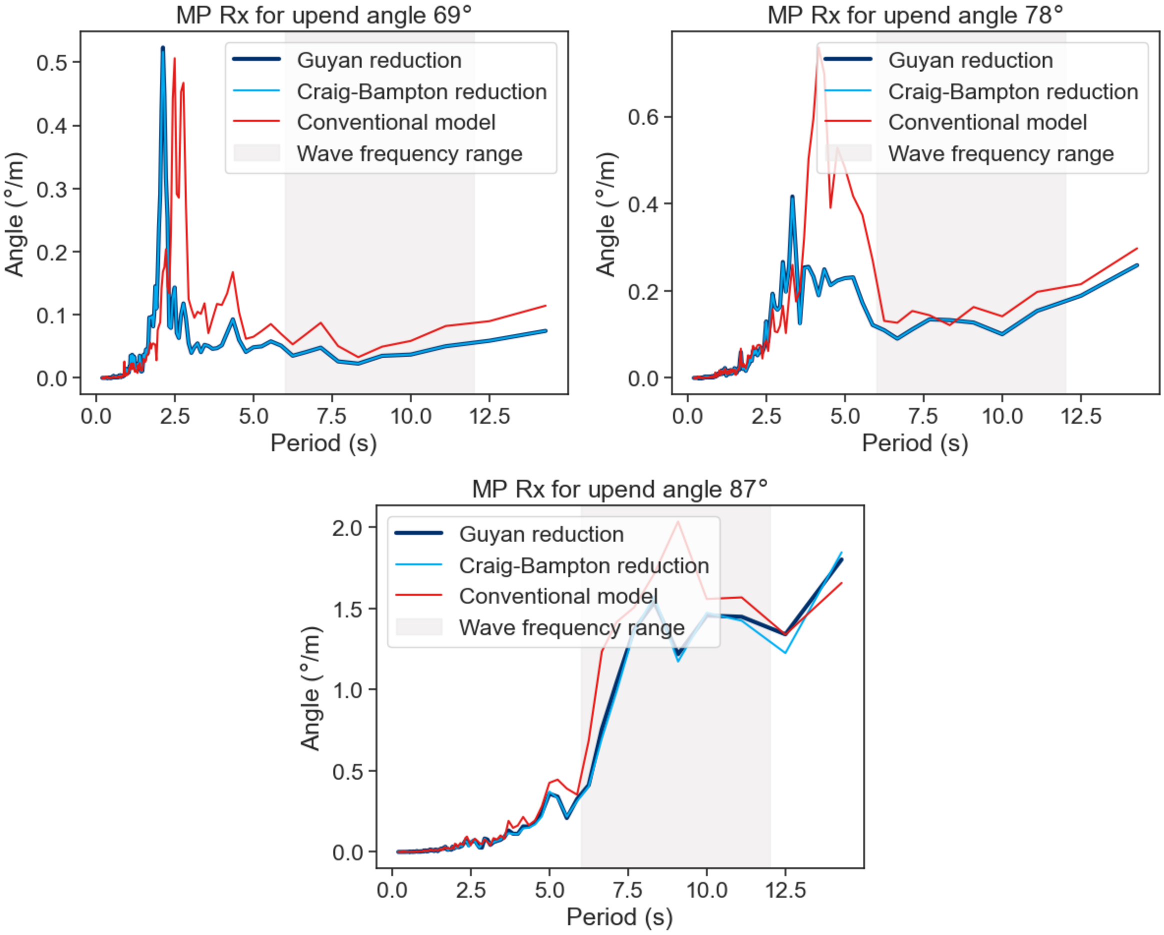

Figure B.4: RAOs of the Rx rotation of the Monopile for the 3 upending angles

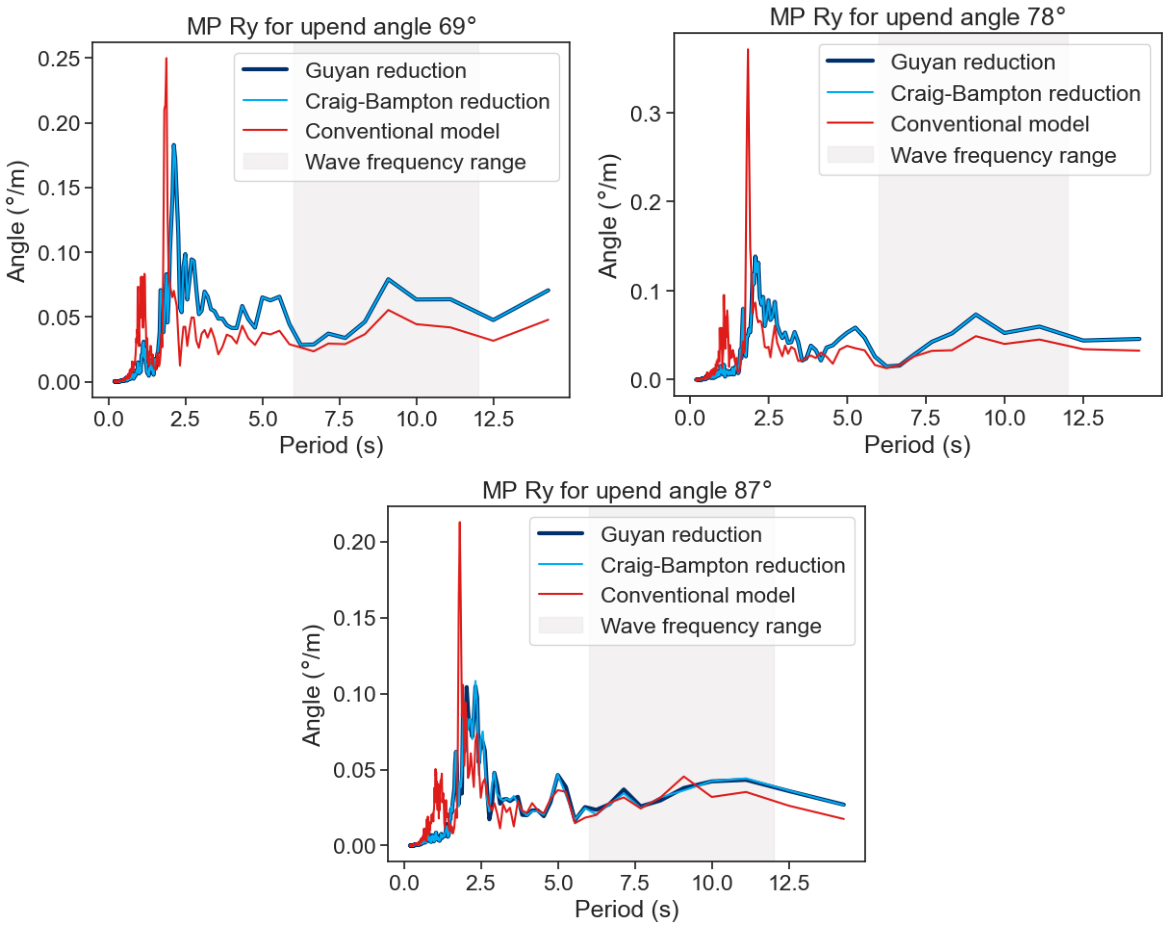

Figure B.5: RAOs of the Ry rotation of the monopile for the 3 upending angles

C

Derivation of the response of a simple system of masses

Below are the derivations of the responses for both ways of modelling the simple system of masses introduced in section 5.2.

Continuous system

```
restart;
```

```
rho*diff(u(x,t),t$2)-E*A*diff(u(x,t),x$2)=0;
u(x,t)=U(x)*e^(i*\omega*t)
```

$$\rho \left(\frac{\partial^2}{\partial t^2} u(x,t) \right) - E\,A \left(\frac{\partial^2}{\partial x^2} u(x,t) \right) = 0$$

$$u(x,t) = U(x)\, e^{i\,\omega\,t} \tag{1}$$

```
-rho*A*U*omega^2-E*A*diff(U(x,t),x$2)=0;
```

$$-\rho\,A\,U\,\omega^2 - E\,A \left(\frac{\partial^2}{\partial x^2} U(x,t) \right) = 0 \tag{2}$$

```
diff(U(x,t),x$2)+U*(omega^2/c^2)=0;
c := sqrt(E/rho);
```

$$\frac{\partial^2}{\partial x^2} U(x,t) + \frac{U\,\omega^2}{c^2} = 0 \tag{3}$$

$$c := \sqrt{\frac{E}{\rho}} \tag{3}$$

```
U := C1*cos(omega*x/c)+C2*sin(omega*x/c);
```

$$U := C1 \cos\left(\frac{\omega\,x}{\sqrt{\frac{E}{\rho}}} \right) + C2 \sin\left(\frac{\omega\,x}{\sqrt{\frac{E}{\rho}}} \right) \tag{4}$$

```
U_prime := diff(U, x):
eq1 := -E*A*eval(U_prime, x=0) = m*omega^2*eval(U, x=0)+F0-k1*(eval(U,
x=0)-eval(U, x=L))-I*omega*c1*(eval(U, x=0)-eval(U, x=L));
eq2 := E*A*eval(U_prime, x=L) = -k1*(eval(U, x=L)-eval(U, x=0))-I*
omega*c1*(eval(U, x=L)-eval(U, x=0));
```

$$eq1 := -\frac{E\,A\,C2\,\omega}{\sqrt{\frac{E}{\rho}}} = m\,\omega^2\,C1 + F0 - k1 \left(C1 - C1 \cos\left(\frac{\omega\,L}{\sqrt{\frac{E}{\rho}}} \right) - C2 \sin\left(\frac{\omega\,L}{\sqrt{\frac{E}{\rho}}} \right) \right)$$
$$- \mathrm{I}\,\omega\,c1 \left(C1 - C1 \cos\left(\frac{\omega\,L}{\sqrt{\frac{E}{\rho}}} \right) - C2 \sin\left(\frac{\omega\,L}{\sqrt{\frac{E}{\rho}}} \right) \right)$$

$$eq2 := E\,A \left(-\frac{C1\,\omega \sin\left(\frac{\omega\,L}{\sqrt{\frac{E}{\rho}}} \right)}{\sqrt{\frac{E}{\rho}}} + \frac{C2\,\omega \cos\left(\frac{\omega\,L}{\sqrt{\frac{E}{\rho}}} \right)}{\sqrt{\frac{E}{\rho}}} \right) = -k1 \left(C1 \cos\left(\frac{\omega\,L}{\sqrt{\frac{E}{\rho}}} \right) \right. \tag{5}$$

$$+ C2 \sin\left(\frac{\omega L}{\sqrt{\frac{E}{\rho}}}\right) - C1\Bigg) - \mathrm{I}\,\omega\, c1 \left(C1 \cos\left(\frac{\omega L}{\sqrt{\frac{E}{\rho}}}\right) + C2 \sin\left(\frac{\omega L}{\sqrt{\frac{E}{\rho}}}\right) - C1\right)$$

```
solve({eq1, eq2}, {C1, C2}):
U_solved := subs(%, U):
U_substituted := subs({
L=3,
rho=8000,
A=0.01,
E=4E3,
k1=200,
c1=10,
m=1000000,
x=3,
omega=1/T
},
U_solved):

RAO := abs(U_substituted/F0):
phase := arctan(Im(U_substituted/F0)/Re(U_substituted/F0)):

evalf(subs(T=10, RAO));
```

$$0.0001005486849 \qquad \textbf{(6)}$$

```
with(plottools):
plot1 := plot(RAO, T=0..20);
data := getdata(plot1)[3]:
Export("continuous.csv", data):
```

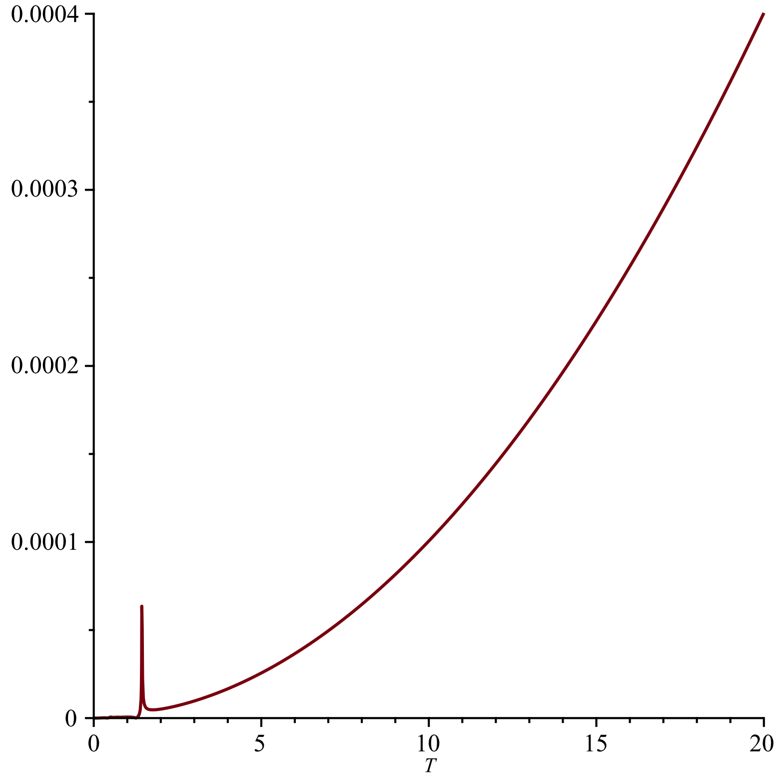

```
plot(phase, T=0..20)
```

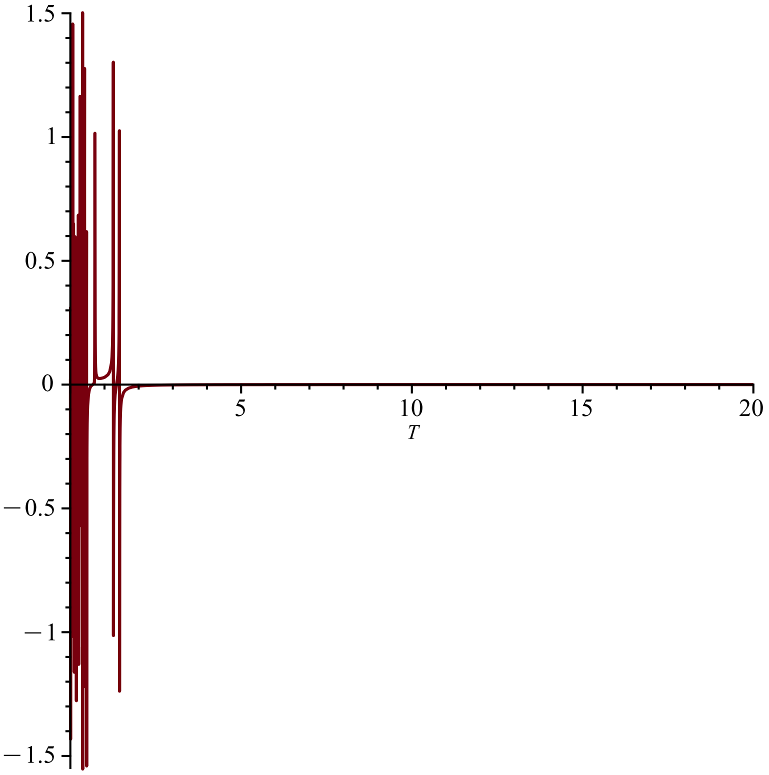
1.5
1
0.5
0
− 0.5
− 1
− 1.5
5
10
15
20
T

Snipped system

```
restart;
rho*diff(u(x,t),t$2)-E*A*diff(u(x,t),x$2)=0;
u(x,t)=U(x)*e^(i*\omega*t)
```

$$\rho \left(\frac{\partial^2}{\partial t^2} u(x,t) \right) - E\, A \left(\frac{\partial^2}{\partial x^2} u(x,t) \right) = 0$$

$$u(x,t) = U(x)\, e^{i\,\omega\,t} \tag{1}$$

```
-rho*A*U*omega^2-E*A*diff(U(x,t),x$2)=0;
```

$$-\rho\, A\, U\, \omega^2 - E\, A \left(\frac{\partial^2}{\partial x^2} U(x,t) \right) = 0 \tag{2}$$

```
diff(U(x,t),x$2)+U*(omega^2/c^2)=0;
c := sqrt(E/rho);
```

$$\frac{\partial^2}{\partial x^2} U(x,t) + \frac{U\, \omega^2}{c^2} = 0$$

$$c := \sqrt{\frac{E}{\rho}} \tag{3}$$

```
U1 := C1*cos(omega*x1/c)+C2*sin(omega*x1/c);
U2 := C3*cos(omega*x2/c)+C4*sin(omega*x2/c);
```

$$U1 := C1 \cos\left(\frac{\omega\, x1}{\sqrt{\frac{E}{\rho}}} \right) + C2 \sin\left(\frac{\omega\, x1}{\sqrt{\frac{E}{\rho}}} \right)$$

$$U2 := C3 \cos\left(\frac{\omega\, x2}{\sqrt{\frac{E}{\rho}}} \right) + C4 \sin\left(\frac{\omega\, x2}{\sqrt{\frac{E}{\rho}}} \right) \tag{4}$$

```
L := 3:
k2 := E*A/(l):
U1_prime := diff(U1, x1):
U2_prime := diff(U2, x2):
eq1 := -E*A*eval(U1_prime, x1=0) = m*omega^2*eval(U1, x1=0)+F0-k1*
(eval(U1, x1=0)-eval(U2, x2=L/2-l/2))-I*omega*c1*(eval(U1, x1=0)-eval
(U2, x2=L/2-l/2));
eq2 := E*A*eval(U2_prime, x2=L/2-l/2) = -k1*(eval(U2, x2=L/2-l/2)-eval
(U1, x1=0))-I*omega*c1*(eval(U2, x2=L/2-l/2)-eval(U1, x1=0));
eq3:= -E*A*eval(U1_prime, x1=L/2-l/2) = k2*(eval(U1, x1=L/2-l/2)-eval
(U2, x2=0));
eq4:= E*A*eval(U2_prime, x2=0) = -k2*(eval(U1, x1=L/2-l/2)-eval(U2,
x2=0));
```

$$eq1 := -\frac{E\,A\,C2\,\omega}{\sqrt{\frac{E}{\rho}}} = m\,\omega^2\,C1 + F0 - k1\left(C1 - C3\cos\left(\frac{\omega\left(\frac{3}{2}-\frac{l}{2}\right)}{\sqrt{\frac{E}{\rho}}}\right) - C4\sin\left(\frac{\omega\left(\frac{3}{2}-\frac{l}{2}\right)}{\sqrt{\frac{E}{\rho}}}\right)\right) - \mathrm{I}\,\omega\,c1\left(C1 - C3\cos\left(\frac{\omega\left(\frac{3}{2}-\frac{l}{2}\right)}{\sqrt{\frac{E}{\rho}}}\right) - C4\sin\left(\frac{\omega\left(\frac{3}{2}-\frac{l}{2}\right)}{\sqrt{\frac{E}{\rho}}}\right)\right)$$

$$eq2 := E\,A\left(-\frac{C3\,\omega\sin\left(\frac{\omega\left(\frac{3}{2}-\frac{l}{2}\right)}{\sqrt{\frac{E}{\rho}}}\right)}{\sqrt{\frac{E}{\rho}}} + \frac{C4\,\omega\cos\left(\frac{\omega\left(\frac{3}{2}-\frac{l}{2}\right)}{\sqrt{\frac{E}{\rho}}}\right)}{\sqrt{\frac{E}{\rho}}}\right) = -k1\left(C3\cos\left(\frac{\omega\left(\frac{3}{2}-\frac{l}{2}\right)}{\sqrt{\frac{E}{\rho}}}\right) + C4\sin\left(\frac{\omega\left(\frac{3}{2}-\frac{l}{2}\right)}{\sqrt{\frac{E}{\rho}}}\right) - C1\right) - \mathrm{I}\,\omega\,c1\left(C3\cos\left(\frac{\omega\left(\frac{3}{2}-\frac{l}{2}\right)}{\sqrt{\frac{E}{\rho}}}\right) + C4\sin\left(\frac{\omega\left(\frac{3}{2}-\frac{l}{2}\right)}{\sqrt{\frac{E}{\rho}}}\right) - C1\right)$$

$$eq3 := -E\,A\left(-\frac{C1\,\omega\sin\left(\frac{\omega\left(\frac{3}{2}-\frac{l}{2}\right)}{\sqrt{\frac{E}{\rho}}}\right)}{\sqrt{\frac{E}{\rho}}} + \frac{C2\,\omega\cos\left(\frac{\omega\left(\frac{3}{2}-\frac{l}{2}\right)}{\sqrt{\frac{E}{\rho}}}\right)}{\sqrt{\frac{E}{\rho}}}\right) = \frac{E\,A\left(C1\cos\left(\frac{\omega\left(\frac{3}{2}-\frac{l}{2}\right)}{\sqrt{\frac{E}{\rho}}}\right) + C2\sin\left(\frac{\omega\left(\frac{3}{2}-\frac{l}{2}\right)}{\sqrt{\frac{E}{\rho}}}\right) - C3\right)}{l}$$

$$eq4 := \frac{E\,A\,C4\,\omega}{\sqrt{\frac{E}{\rho}}} = -\frac{E\,A\left(C1\cos\left(\frac{\omega\left(\frac{3}{2}-\frac{l}{2}\right)}{\sqrt{\frac{E}{\rho}}}\right)+C2\sin\left(\frac{\omega\left(\frac{3}{2}-\frac{l}{2}\right)}{\sqrt{\frac{E}{\rho}}}\right)-C3\right)}{l} \tag{5}$$

```
coefficients := solve({eq1, eq2, eq3, eq4}, {C1, C2, C3, C4}):
U1_solved := subs(coefficients, U1):
U2_solved := subs(coefficients, U2):

l1:=L/4:
variables := {
rho=8000,
A=0.01,
E=4E3,
k1=200,
c1=10,
m=1000000,
l=l1,
omega=1/T,
x1=0,
x2=L/2-l1}:

U1_substituted := subs(variables, U1_solved):
U1_re := Re(U1_substituted/F0):
U1_im := Im(U1_substituted/F0):
U2_substituted := subs(variables, U2_solved):
U2_re := Re(U2_substituted/F0):
U2_im := Im(U2_substituted/F0):

RAO1 := evalf(sqrt(U1_re^2+U1_im^2)):
phase1 := evalf(arctan(U1_im/U1_re)):
RAO2 := evalf(sqrt(U2_re^2+U2_im^2)):
phase2 := evalf(arctan(U2_im/U2_re)):
evalf(subs(T=10, RAO2));

with(plottools):
plot1 := plot(RAO2, T=0..20);
data := getdata(plot1)[3]:
Export("snipped.csv", data):
```

```
0.0001010670132
```

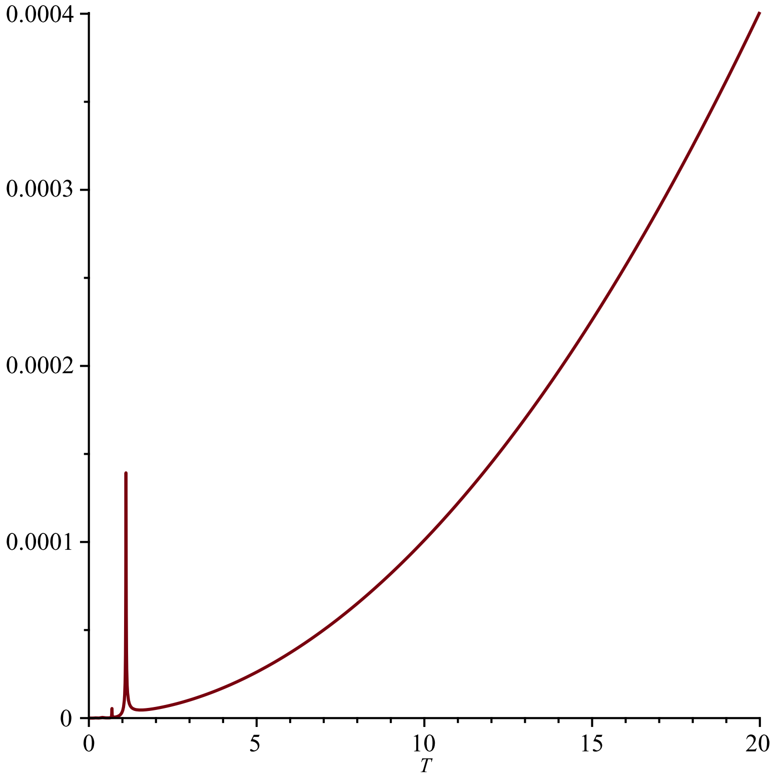

```
plot(phase2, T=0..10);
```

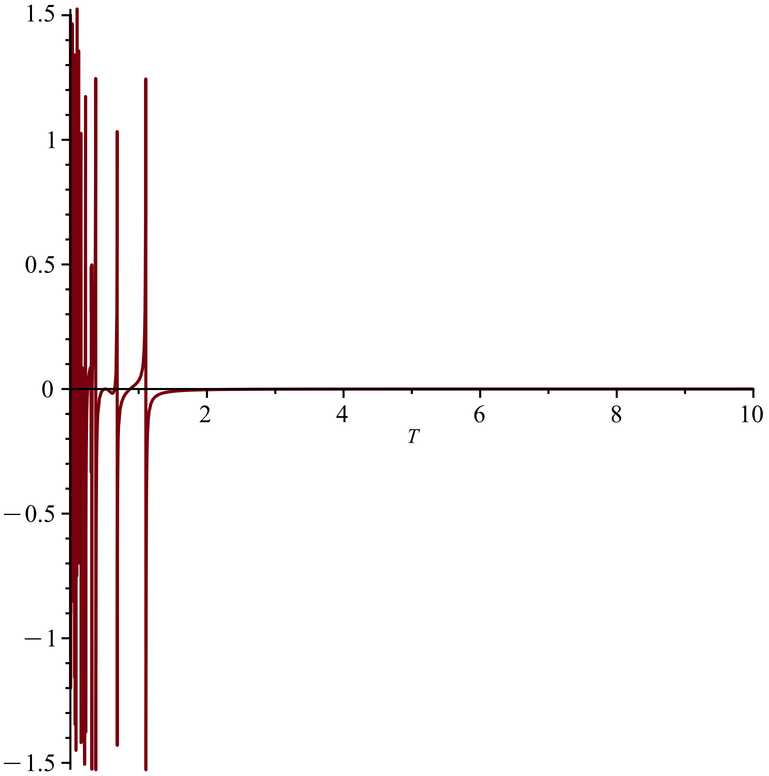
1.5
1
0.5
0
−0.5
−1
−1.5
2
4
6
8
10
T